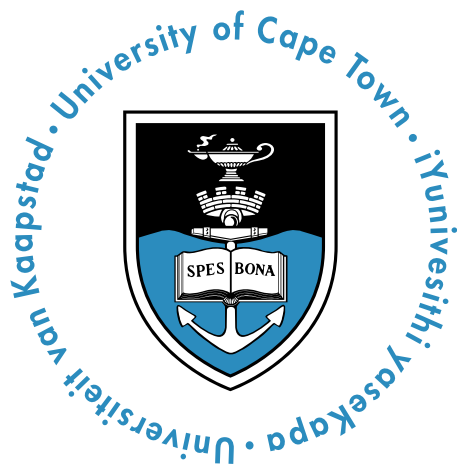


# RADAR SIGNAL PROCESSING FOR TRAFFIC CALMING RADAR APPLICATIONS

---



Presented by:

Salmaan Kamaloodien

Prepared for:

Dr. Yunus Abdul Gaffar

November 6, 2021

Submitted to the Department of Electrical Engineering at the University of Cape Town in partial fulfilment of the academic requirements for the degree of Bsc Mechatronics Eng..

# Abstract

An attempt of using a **CW** S-band radar for traffic calming purposes was made, where evaluation and comparison of the **CA-CFAR** to **CFAR** techniques were done, but no further research was conducted to find the optimal input parameter values in **CA-CFAR** and the **STFT**. As a continuation, research was done to find these optimal values by performing an initial theoretical investigation on the effects of varying the input parameter values. This also assisted in choosing optimal parameter values. Some effects were then experimented on as well as the chosen values being evaluated. Experiments were performed on multiple sized vehicles, driving towards and away from the radar, where results were evaluated based on the speed detected, missed targets and false alarms. Acceptable results were found at speeds less than 45km/h, however at higher speeds inaccuracies were seen, usually estimated as 10km/h less than the true speed. By examining the results, it was observed that the detections were accurately made based on the target locations in the spectrograms. Minimal false alarms were detected while still maintaining acceptable target detection. It was observed that targets with a smaller **RCS** were missed at far distances from the radar. It was concluded that acceptable performance was seen of the **CA-CFAR** process. Further investigation needs to take place to assess the viability of implementing the mobile S-band radar, specifically in capturing data.

# Acknowledgments

Firstly, I would like to say thank you to Allah for the blessing of life, opportunity and ability to achieve all that I have achieved and will achieve in the future.

I would like to thank my supervisor (a lot), Dr. Yunus Abdul Gaffar. Thank you for all that you have taught me, not just regarding this project but in other courses as well. Thank you for the resources you have provided for me, the timely feedback to all my questions, the weekly meetings and the highly appreciated feedback.

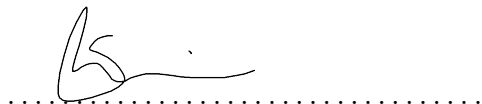
I would also like to thank all my friends that were supporting me throughout university. Specifically Azhar, Crystal, Taqi, Trivaan, Kavir, Sameera and my cat for the company when working on this report, helping me stay awake and focused. Thanks you goes out to Hassa and Jhoana for helping with the word parts of the report, and all others that assisted. As well as Zubair with help in the selection process.

A special thanks for my parents for providing me with the opportunity to study at UCT and for the support, and to my brother.

I would like to extend gratitude to Ferial, for unknowingly providing me with a great foundation to continue research on, as well as the data sets used in the report.

# Plagiarism Declaration

1. I know that plagiarism is wrong. Plagiarism is to use another's work and pretend that it is one's own.
2. I have the IEEE convention for citation and referencing. Each contribution to, and quotation in, this final year project report from the work(s) of other people, has been attributed and has been cited and referenced.
3. This final year project report is my own work.
4. I have not allowed, and will not allow, anyone to copy my work with the intention of passing it off as their own work or part thereof.



Salmaan Kamaloodien

November 6, 2021

Word count: 9962

# Contents

<b>Abstract</b>	i
<b>Acknowledgments</b>	ii
<b>Plagiarism Declaration</b>	iii
<b>Glossary of Abbreviations</b>	iv
<b>Table of Contents</b>	vi
<b>List of Figures</b>	x
<b>List of Tables</b>	xiii
<b>List of Code Listings</b>	xiv
<b>Chapter 1: Introduction</b>	1
1.1 Introduction . . . . .	1
1.2 Background . . . . .	3
1.3 Purpose . . . . .	3
1.3.1 Problem Statement . . . . .	3
1.3.2 Objectives . . . . .	5
1.3.3 Exclusions . . . . .	5
1.3.4 Limitations . . . . .	5

1.4	Outline . . . . .	6
<b>Chapter 2:</b>	<b>Theory</b>	<b>7</b>
2.1	Radar concepts . . . . .	7
2.1.1	Radar Basics . . . . .	7
2.1.2	Frequency Bands . . . . .	8
2.1.3	Signal Power . . . . .	8
2.2	Short Time Frequency Domain . . . . .	11
2.3	Target Detection: Constant False Alarm Rate . . . . .	17
2.3.1	Probability of False Alarm . . . . .	17
2.3.2	Cell Averaging . . . . .	18
2.3.3	Guard Cells . . . . .	19
2.3.4	Threshold . . . . .	20
<b>Chapter 3:</b>	<b>Literature Review</b>	<b>22</b>
3.1	Traffic calming and Road Surveillance . . . . .	22
3.2	Effectiveness of traffic calming . . . . .	23
3.3	Speed reduction and monitoring . . . . .	23
3.3.1	Other methods . . . . .	25
3.3.2	Radar methods . . . . .	26
3.4	Proposed method . . . . .	29
3.4.1	Radar Testing . . . . .	30
3.4.2	Target Detection . . . . .	31
3.4.3	Results . . . . .	32
3.4.4	Work Omitted . . . . .	35
<b>Chapter 4:</b>	<b>Methodology</b>	<b>36</b>
4.1	Approach . . . . .	36
4.2	Literature and Theory . . . . .	36

4.3	Simulation . . . . .	37
4.4	Experimental procedure . . . . .	37
4.4.1	Procedure . . . . .	38
4.4.2	Validation . . . . .	41
4.4.3	Process Summary . . . . .	42
<b>Chapter 5:</b>	<b>Design</b>	<b>44</b>
5.1	Validation . . . . .	44
5.2	Implementation . . . . .	45
5.2.1	Short Time Fourier . . . . .	45
5.2.2	Target Detection . . . . .	48
5.2.3	Speed Detection . . . . .	49
5.3	Experimentation . . . . .	49
5.3.1	Considerations . . . . .	49
5.3.2	Coherent Processing Interval . . . . .	50
5.3.3	Overlap Factor . . . . .	51
5.3.4	Window Shape . . . . .	53
5.3.5	Probability of False Alarm . . . . .	53
5.3.6	Reference window . . . . .	53
5.3.7	Guard cells . . . . .	54
5.3.8	Parameter choices summary . . . . .	54
5.3.9	Evaluation . . . . .	55
<b>Chapter 6:</b>	<b>Results</b>	<b>56</b>
6.1	Validation . . . . .	56
6.2	Experimentation . . . . .	59
6.2.1	Coherent Processing Interval . . . . .	60
6.2.2	Probability of False Alarm . . . . .	61

6.2.3	Reference Window . . . . .	62
6.3	Decided parameter value . . . . .	63
6.3.1	Audi . . . . .	64
6.3.2	Lexus . . . . .	65
6.3.3	Bike . . . . .	66
6.3.4	Multi-target Detection . . . . .	68
<b>Chapter 7:</b>	<b>Conclusions</b>	<b>70</b>
7.1	Conclusions . . . . .	70
7.2	Future Work . . . . .	71
<b>Bibliography</b>		<b>73</b>
<b>Appendix A:</b>	<b>Code</b>	<b>77</b>
A.1	Code . . . . .	77
<b>Appendix B:</b>	<b>More Data sets</b>	<b>78</b>
B.1	Audi . . . . .	79
B.2	Lexus . . . . .	80
B.2.1	Bike . . . . .	81
B.2.2	Multi-target . . . . .	81

# List of Figures

1.1	Display of traffic calming radar, provided by [3]	2
2.1	Frequency band divisions and some commercial uses [9]	8
2.2	A visualisation of the Doppler effect [11]	10
2.3	Short Time Fourier Transform done on an arbitrary signal $x(t)$ [12]	12
2.4	The spectrum of the STFT done with a low CPI vs a high CPI, where other parameters are kept constant.	14
2.5	Overlap between two consecutive windows	15
2.6	Representation of window signals in the time and frequency domain	16
2.7	Cell structure used in computing the CA-CFAR threshold	17
2.8	Probability Density Function (PDF) of Noise signal (left) and noise+target (right) plotted, effect of threshold shown	18
2.9	The peak of a signal spanning over more than one cell	19
2.10	Threshold plotted against a signal with a target detected.	20
3.1	Traffic circle used to reduce speed, implemented in Addis Ababa, Ethiopia.	24
3.2	Magnetic loops used in vehicle detection [22]	25
3.3	Set up of Single Side looking Radar [25]	27
3.4	TC-400 radar display by RadarSign [3].	29
3.5	The results of testing the constructed radar [6]	31

3.6	Generated spectrogram between cases of smallest and biggest ROC measured [6] . . . . .	33
3.7	Summaries results from the experiments performed [6] . . . . .	34
4.1	The completed radar used to measure data, provided by [6] . . . . .	39
4.2	The experimental setup used when measuring data . . . . .	40
4.3	Summary of the methodology used to develop and execute the investigation. . . . .	43
5.1	The performance of a Hanning window with regards to the % overlap [14]	52
6.1	Example of generated Data . . . . .	57
6.2	Generated Chirp signal used to test the spectrogram algorithm . . . . .	58
6.3	Target Detected in Simulated noise+target . . . . .	58
6.4	Target location marked in simulated signal of target in noise . . . . .	59
6.5	The set up of the radar and Audi a1 used in capturing the data used in comparisons. . . . .	60
6.6	The difference of targets detected for the Audi A1 driving away at 30km/h of CPI=0.6 vs. CPI=0.8 . . . . .	61
6.7	The difference of targets detected for the Audi A1 driving away at 30km/h of PFA= $10^{-14}$ vs. PFA= $10^{-50}$ . . . . .	62
6.8	The result found when the size of each reference window was set to 300.	63
6.9	Final speed vs time plots derived from the applied algorithm on the Audi A1 . . . . .	64
6.10	Final speed vs time plots derived from the applied algorithm on the Lexus . . . . .	65
6.11	scale=0.6 . . . . .	66
6.12	Final speed vs time plots derived from the applied algorithm on the Motorbike . . . . .	67

6.13	The spectrogram resulting from '03_Motorbike_Driving_Towards_60KPH_001.wav'	68
6.14	Spectrogram generated from '11_Bremner_Lexus_InfrontOf_PoloGtI_Driving_Towards_60KPH_001.wav'	69
B.1	Spectograms generated from the Audi data set . . . . .	79
B.2	All generated spectrograms of Lexus Bremner. . . . .	80
B.3	Spectrograms generated from the Bike data . . . . .	81
B.4	Spectrograms generated from recordings when two vehicles passed . .	81

# List of Tables

3.1	Comparison of CFAR techniques [6] . . . . .	32
4.1	Input parameters varied in STFT and Spectrogram . . . . .	42
4.2	Input parameters varied in CA-CFAR . . . . .	42
5.1	Chosen parameter values that were used . . . . .	55
6.1	Chosen parameter values that were used . . . . .	63
6.2	Speed detection results for the Audi A1 . . . . .	64
6.3	Speed detection results for the Lexus 4x4 . . . . .	65
6.4	Speed detection results for the motorbike . . . . .	67

# List of Code Listings

5.1	Code used to prepare data . . . . .	46
5.2	Input Parameters being set . . . . .	46
5.3	Window function preparation . . . . .	47
5.4	Doppler frequency to Speed (km/h) where 'c' is the speed of light. . .	48

# Chapter 1

## Introduction

### 1.1 Introduction

Importance of road safety has always been considered a priority. Various regulations as to what is considered 'Road worthy' are in place. However, road safety does not just end there. Liabilities to safety standards extend to how the car is driven too. Therefore techniques exist which provide a means of safety while the vehicle is on the road. These techniques greatly vary, but all fall under the practice of traffic calming. This can be implemented employing contact, such as speed bumps, as well as non-contact methods, like speed cameras. Both of which make use of many different technologies.

Radar is a commonly explored option used in traffic calming techniques. Many radar techniques allow for a non-contact method to track speed. Compared to other techniques, implementing radar techniques offers an acceptable solution that does not involve installation that may involve the breaking down and rebuilding of roads. Potentially lowering the costs and other requirements. Physical means of traffic calming have been shown to negatively contribute to the wear and tear of vehicles. [1]

Considering the various non-contacts method that may be used, Radar provides a

non-invasive solution. Using sound has the possibility of causing noise pollution and light may introduce some safety concerns, being distracting to the drivers. There is the opportunity to determine both range and speed detection in radar.

There are already existing applications of radar in traffic calming techniques. In Chandler, Arizona, it was shown that the installation of radar speed signs has provided an average speed decrease of 4 mph [2]. A company called RadarSign provides a commercially available solution to residents by offering to install radar speed signs to benefit local street safety [3], this is shown in Fig. 1.1. Repro supplies is another (local) company that sells radar speed detection signs [4].



Figure 1.1: Display of traffic calming radar, provided by [3]

## 1.2 Background

This project is the development of a low-cost radar system to be used in traffic calming applications. This extends to the design of the system as well as the processing techniques required to accurately determine the speed of a passing vehicle. Radar is an extremely versatile technology. Several disciplines make use of radar technology. The first radar was developed to be used in the military field. Radar technologies have since evolved into various fields, including, but not limited to, climatology, communication, and astronomy. [5]

Although there are many reasons for the use of radar in traffic calming applications, there still exists hurdles associated with that implementation. There are usually high costs involved in radar usage. Along with this, there are also some considerations involved with the space requirements of the hardware. Thus, the development of a robust, low-cost traffic calming radar system is needed. This is to be implemented in pedestrian-rich areas, such as school or residential areas to improve awareness and safety.

## 1.3 Purpose

### 1.3.1 Problem Statement

To provide an effective and robust solution with the current implementation, challenges arise:

- Non-invasive speed detection techniques.
- Well-documented radar design that can be adapted into specific use-cases.
- Accurate process to detect targets in radar signals to later be used to determine velocity.

- Low-cost solutions

Solutions to these challenges have been found:

The S-Band radar system designs were provided by the MIT IAP radar course. This device makes use of readily available parts, with suitable documentation for further processing. Thus, it was taken as a suitable test-bed device.

In 2019, work was done to construct the MIT S-band coffee can radar and to perform measurements with various vehicles [6]. Initial results on estimating the speed of the vehicle were presented. It was found that the performance of the S-band radar was acceptable, with an average error of 9.9%. Furthermore, a comparison of different [Constant False Alarm Rate \(CFAR\)](#) processing techniques (CA-CFAR, OS-CFAR, and OSGO-CFAR) was done. The best performance was found in OS-CFAR and the worse in [Cell Averaging-Constant False Alarm Rate \(CA-CFAR\)](#).

However, in [6] insufficient work has been conducted concerning optimum parameters of the radar detection technique on the performance of estimating the speed of a moving vehicle. There is also a deficit in the investigation of the optimum parameters used in the computation of the [Short Time Fourier \(STFT\)](#). Furthermore, results were only shown on a few measured datasets. Implementation of the device as a weatherproof product providing real-time feedback to drivers has not been done.

This report covers the investigation and optimisation of the input parameters used in the [CA-CFAR](#) algorithm used. The parameters used in the [STFT](#) has also been investigated, and findings were included in the report. In addition, results are shown for a wide variety of measured vehicles and one motorbike.

These investigations have the potential to determine the viability of this project more accurately. Furthermore, optimisation could increase the performance of the device used. This would also provide a means to accurately determine the required processing requirements in later stages of the project.

### 1.3.2 Objectives

This project has objectives to:

- Determine optimum parameter values when computing the STFT to aid the radar detection algorithm in the next phase of the processing chain.
- Estimate the instantaneous velocity of the moving object and generate results for a wide variety of different vehicles, both in departing and approaching the radar.

### 1.3.3 Exclusions

The work excludes:

- Exploring different methods to collect data
- The assembly of the Radar device
- The exploration of other algorithms
- Implementation in the final product

### 1.3.4 Limitations

The limitations of the project are as follows:

- 11-week time allocation
- All experimental work to be done in Matlab.

## 1.4 Plan of Development

The remainder of this thesis is organized as follows:

**Chapter 2, Theory:** Fundamental principles of the radar and target techniques implemented

**Chapter 3, Literature review:** Literature review

**Chapter 4, Methodology:** Project methodology

**Chapter 5, Design:** The implementation used to conduct validation and perform the experiments

**Chapter 6, Results:** Explore and discuss the results achieved

**Chapter 7, Conclusion:** Conclusion and further recommendations

# Chapter 2

## Theory

In this chapter related theory behind the approach has been explained. Fundamental Radar theory concerning measurements, processing, and target detection has been elaborated on.

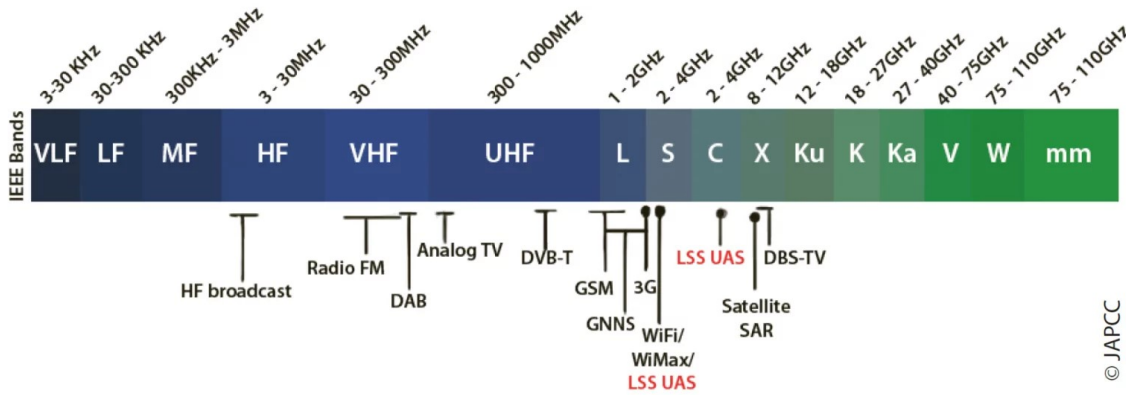
### 2.1 Radar concepts

#### 2.1.1 Radar Basics

The concept of radar is based on Radio Frequencies (RF) Electromagnetic (EM) waves. The EM waves are transmitted towards an object. Next, the signal is reflected by the object and transmitted back to the receiver. However, unwanted EM waves are present in any environment, which the receiver will still measure [7]. Two radar types are considered; Continuous wave (CW) and pulse-doppler. Measurements to determine speed were made in CW mode, as this has allowed for measurements of varying frequency. For range detection methods pulse-doppler radar systems are used [7], however, this is outside the scope of this report.

### 2.1.2 Frequency Bands

Different radio frequency usages operates across a wide range. The IEEE standard has divided this range into bands, each represented by a letter [8]. A portion of the spectrum is shown in Fig. 2.1, as well as some commercial uses corresponding with specific bands.



© JAPCC

Figure 2.1: Frequency band divisions and some commercial uses [9]

The radar used to measure the data was operational in the S-band. Fig. 2.1 show that it will have a frequency range between 2-4GHz.

### 2.1.3 Signal Power

A signal is transmitted at a specified power, thus the reflected signal will be of a higher magnitude than noise present. The difference between the signal and that of the noise is expressed as a ratio, called the Signal to Noise Ratio (SNR) shown in Eq: 2.1 [7].

$$SNR = \frac{P_r}{P_n} \quad (2.1)$$

Loss in signal power based on the distance the signal travels, governed by Equation 2.2 (in mono-static configuration), is often referred to as 'The Radar Equation' [7].

$$P_r = \frac{P_t G_t \sigma}{(4\pi)^2 R^4} \quad (2.2)$$

In Fig. 2.2:

- $P_r$ : Power of the received signal at the antenna.
- $P_t$ : Power of the signal transmitted.
- $G_t$ : Transmit gain (the intensity of the signal in the direction of transmission)
- $\sigma$ : Cross sectional area of the radar ( $m^2$ )
- $R$ : Distance between target and receiver/antenna.

Therefore, it can be seen that the signal power of large moving targets with a high Radar Cross-Section (RCS), typically greater than  $1m^2$  would result in being much than that reflected by the background noise [10], [7]. Allowing for signal detection.

### Electromagnetic Interference

In radar, there are undesired sources of EM waves. These have resulted from environmental sources such as Wireless communication technologies used in the vicinity of measurements taken or clutter from unwanted reflections. Internal sources of interference also exist, caused by internal circuitry [7].

### Doppler Shift

Doppler effect describes the relationship between speed and a changing frequency. This is when the radar signal is reflected off a target is has been compressed or

expanded based on the relative radial velocity of the target to the signal as shown in Fig. 2.2. On the image shown first both cars are stationary, the outgoing waves are seen at a constant wavelength, thus a constant frequency. No difference between the reflected frequency is seen. The second part of the image shows the vehicle has began to approach the radar at a velocity. This velocity causes the reflected signal to be compressed, this will increase frequency.

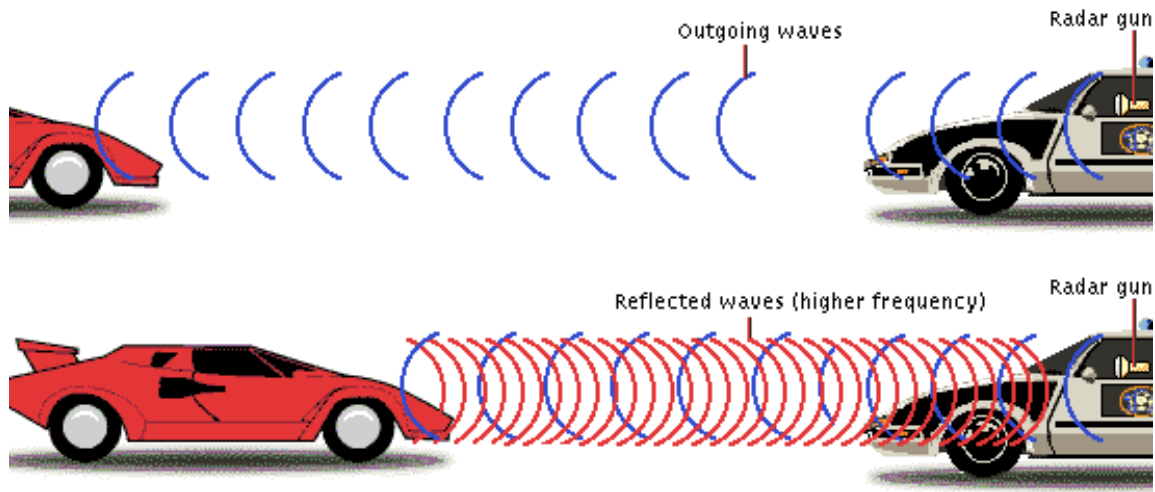


Figure 2.2: A visualisation of the Doppler effect [11]

The detected frequency is directly proportional to the speed, and can be converted as shown in Equation 2.3. Applying this in the STFT will allow speed to be directly derived from the spectrogram.

$$v_r = \frac{c f_d}{2 f_t} \quad (2.3)$$

In Equation 2.3:

- $v_r$ : Velocity of target.
- $f_d$ : Doppler frequency.

- $c$ : Speed of light.
- $f_t$ : Centre frequency transmitted by the radar.

## 2.2 Short Time Frequency Domain

To perform adequate frequency analysis of a signal with respect to time the **STFT** has to be applied. Direct Fourier transform provides the spectrum for the signal as a whole, without a temporal resolution [12].

To compute the **STFT** a window function needs to be made. Window functions or Frames are often used to isolate a subset of the data available. 'Windowing' refers to the process of applying a window on a signal.

In the frequency domain, windowing is often used for demodulation or eliminating artefacts. In the time domain, windowing is often used to compute the **STFT** [7].

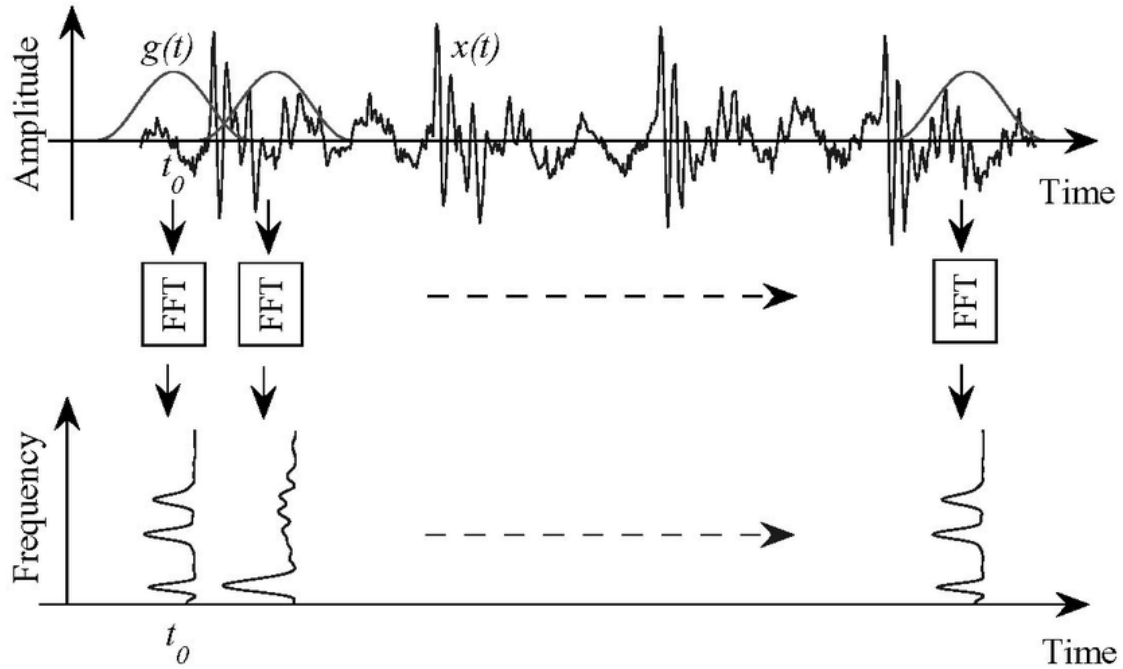


Figure 2.3: Short Time Fourier Transform done on an arbitrary signal  $x(t)$  [12]

In Fig. 2.3 the effect on windowing can be observed. The window function extracts a sub-sample of the signal. Subsequently, the **Fast Fourier Transform (FFT)** is applied. The window then slides to the next location extracting another sample, **FFT** is applied once again. This process is repeated over the whole signal. It is also noted that for each window the **FFT** is plotted as a 3-D output with respect to time.

$$X_m(\omega) = \sum_{n=0}^N x(n)g(n - mR)e^{-j\omega n} \quad (2.4)$$

Equation 2.4 represents a mathematical expression of the **STFT** shown in Fig. 2.3, but as a function of discrete time [13]. This shows the **Discrete Time Fourier Transform (DTFT)** being applied at a specific window applied to the input signal, where:

- $X_m(\omega)$ : Frequency spectrum at time  $mR$  (mth window applied to the signal)
- $N$ : Number of samples in the input signal
- $x(n)$ : Discrete time input signal of time  $n$
- $g(n)$ : Window function, of specified length.
- $R$ : Hop size, in samples.

Aspects of the window function that are looked at when processing time-based signals are the [Coherent Processing Interval \(CPI\)](#), [Overlap Factor \(OLF\)](#) and the window function. Considerations are to be made with the trade-off between the temporal and frequency resolution [12].

### [Coherent Processing Interval](#)

'[Coherent Processing Interval \(CPI\)](#)' refers to the interval over which the window function is applied. This is used to determine the number of samples within a frame [7].

It is often desired to minimize the magnitude of the [CPI](#), as this will provide a higher resolution when observing variations for the Doppler frequency. However, this decrease results in a lower frequency resolution. This trade-off between temporal and frequency is attributed to the localization in the frequency axis that comes with a narrower width [13].

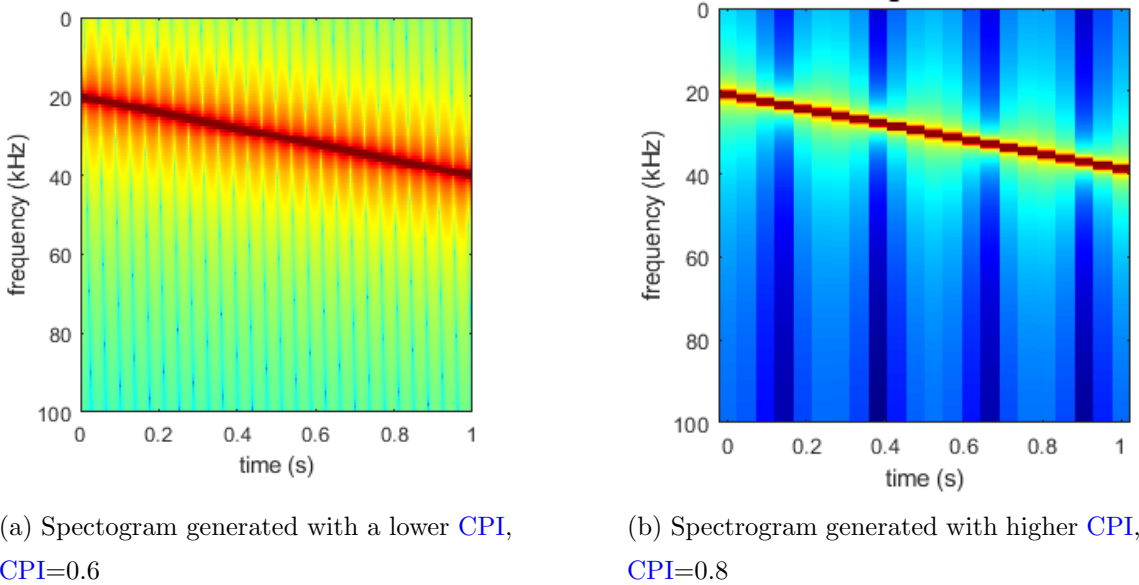


Figure 2.4: The spectrum of the STFT done with a low CPI vs a high CPI, where other parameters are kept constant.

In Fig. 2.4 the comparison of a low CPI vs a high CPI can be seen, for an arbitrary chirp signal. Where the high CPI, Fig. 2.4b, shows a clearer frequency axis, but the temporal resolution can be seen as jagged, compared to the low CPI, Fig. 2.4a, where it shows the opposite.

### Overlap Factor

**Overlap Factor (OLF)** describes the factor by which two consecutive frames overlap. This contributes to the number of samples or duration between each frame, often referred to as the hop. Overlap is generally applied as a method of combatting the temporal losses associated with a wider frame. Often it is desired to have a high **Overlap Factor**. However, this will come at computational costs, as well as high-frequency signals being amplified more than that of lower [14].

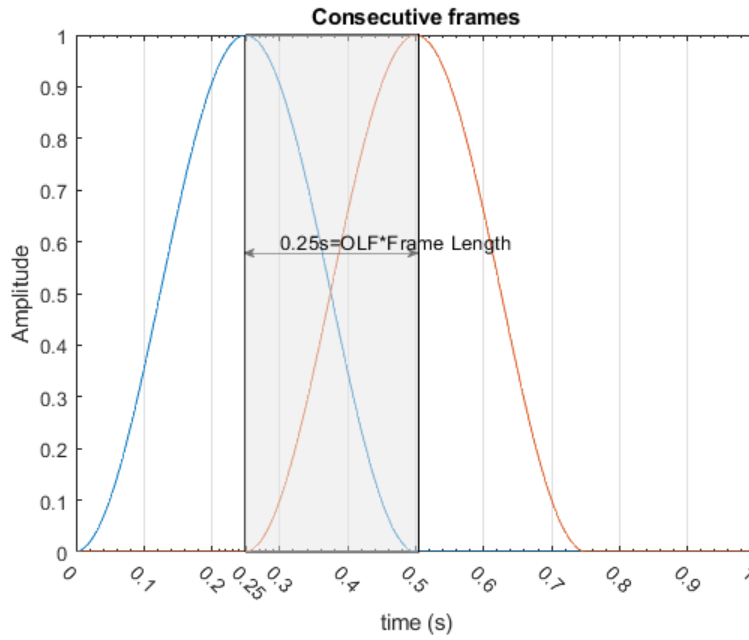


Figure 2.5: Overlap between two consecutive windows

Fig. 2.5 shows the overlap between two consecutive windows. The length of the overlap shown is calculated in Equation 2.5, where the **Overlap Factor** is shown as the amount of overlap relative to the frame size.

$$\text{Overlap} = \text{OLF} * \text{FrameLength} \quad (2.5)$$

### Window Shape

The shape of the Window function is often varied based on the requirements of a signal. Window shapes are chosen based on the signal in question. The shape will often determine the representation of the data in the spectrogram. When looking at window functions aspects of the side lobe width, tapering and frequency resolution loss are looked at. These are chosen to reduce the effects of the trade-off often faced

in the **STFT** [14].

Some window functions available are the Hanning, Rectangular, Blackman, and Triangular. The difference in shape has been shown in Fig. 2.6a. The attenuation of the side lobes in a Hanning window is shown in Fig. 2.6b, the attenuation varies in the choice of window function made. Both of what is shown in 2.6 is looked at when determining which function to use.

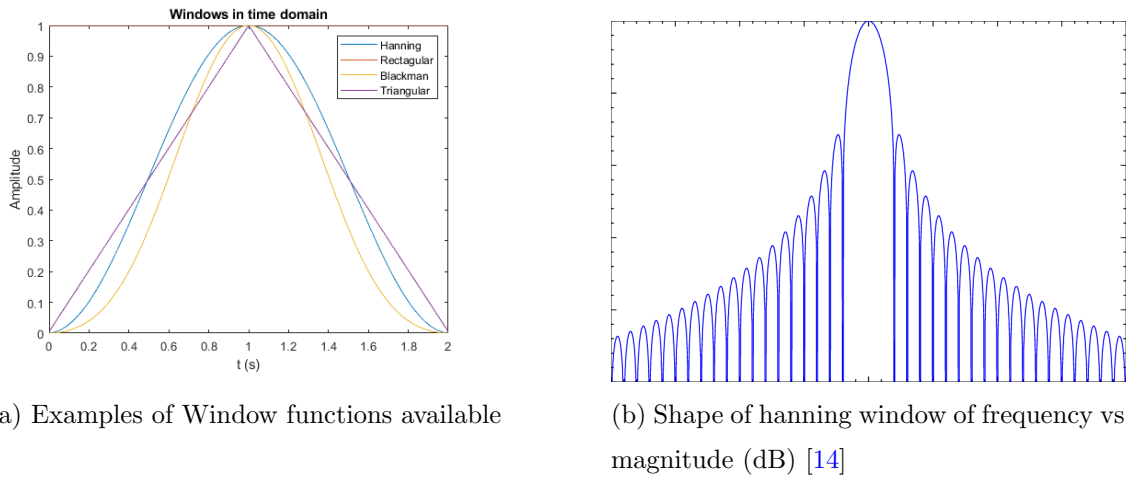


Figure 2.6: Representation of window signals in the time and frequency domain

## Spectrogram

To visualise the **STFT** a spectrogram is used. This is often represented as seen in Fig. 2.4. Each window function applied represents is analogous with a time instance. The power is represented as a colour, in this report Equation 2.6 was used to determine the power of the signal in (dB), where  $Y(\omega, m)$  represents the power.

$$Y(\omega, m) = 20 \log_{10}(|X_m(\omega)|) \quad (2.6)$$

## 2.3 Target Detection: Constant False Alarm Rate

The target detection algorithm implemented makes use of a threshold to determine if a target exists at a frequency. This threshold value has fluctuated based on the signal. The samples that were used within testing are referred to as cells and are divided as shown in Fig. 2.7. The threshold was computed to determine if a target exists in the **Cell Under Test (CUT)**.

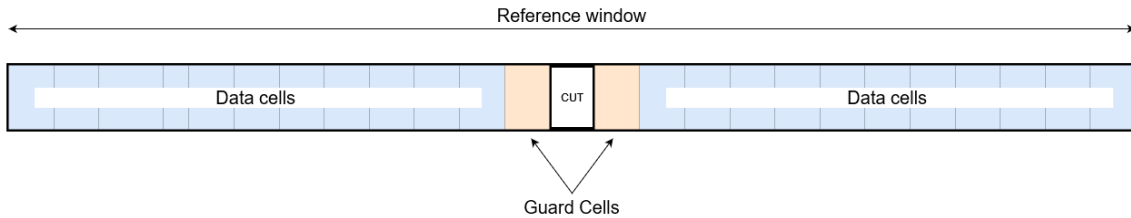


Figure 2.7: Cell structure used in computing the **CA-CFAR** threshold

In Fig. 2.7 the composition of the window used in the **CA-CFAR** is shown. The data cells are coloured blue, and the guard cells are green. The **CUT** is seen the cell being evaluated.

### 2.3.1 Probability of False Alarm

**CFAR** processes make use of statistical estimates of interference to maintain a CFAR, hence a constant **Probability of False Alarm (PFA)**. Thus, the threshold would increase with increased interference. Resulting in a decreased probability of detection ( $P_D$ ). The relationship between the threshold and the **PFA** and  $P_D$  is shown in Fig. 2.8. It is observed that the threshold increase (translate left) would cause a decrease in  $P_D$  (greyed out) and **PFA** (blacked out). Thus, the value of the threshold would need to be minimized while minimizing the **PFA** [7]. The threshold line translates left when the value is increased, this will lessen the  $P_D$  but also lessen the **PFA**. This shows that the magnitude of the threshold is determined by the desired **PFA**.

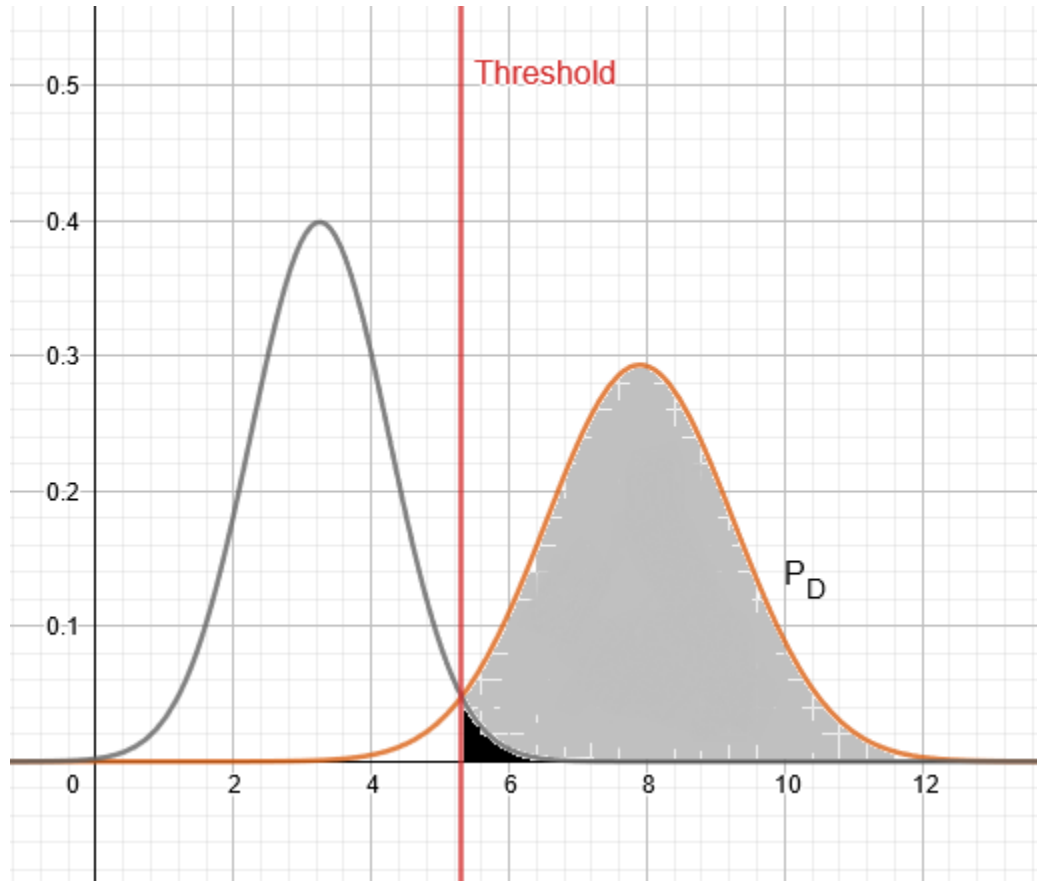


Figure 2.8: Probability Density Function (PDF) of Noise signal (left) and noise+target (right) plotted, effect of threshold shown

The noise was taken in as a Rayleigh distribution and passed through a square-law detector, which has converted the noise to Gaussian, shown in Fig. 2.8.

### 2.3.2 Cell Averaging

Cell Averaging-Constant False Alarm Rate (CA-CFAR) was used to calculate the threshold value [10]. This process was computed in a series of cells, called a reference window this is shown in Fig. 2.7. The mean value of the signal seen in the data cells ( $\sigma^2$ ) was calculated as shown in Equation 2.7. The data cells ( $z_n$ ) were set at

a length( $\frac{N}{2}$ ), symmetrical around the **CUT**. Data cells were also passed through a square-law detector [7].

$$\sigma^2 = \frac{1}{N} \sum_{n=1}^N |z_n|^2 \quad (2.7)$$

A constant ( $\alpha$ ) is calculated based on the **PFA**, as seen in Equation 2.8, assuming that no target is present within the signal [7]. Where N is the length of samples in the reference window shown in Fig. 2.7.

$$\alpha = N[P_{FA}^{-\frac{1}{N}} - 1] \quad (2.8)$$

### 2.3.3 Guard Cells

The guard cells shown in Fig. 2.7 was allocated so that if a target spans more than a single cell, as shown in Fig. 2.9. Guard cells would not be taken into account when evaluating the mean for the threshold calculation [7]. The signal seen in Fig. 2.9 is seen to span over two guard cells on either end. The unseen signal is regarded as noise, the only signal with the target is shown in Fig. 2.9

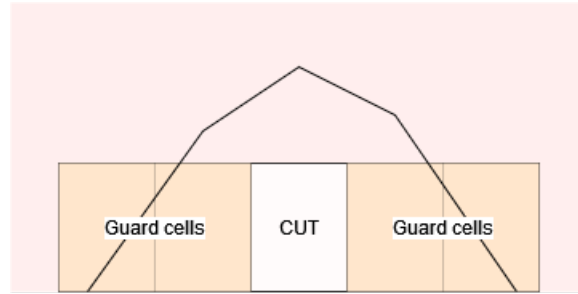


Figure 2.9: The peak of a signal spanning over more than one cell

### 2.3.4 Threshold

The threshold was calculated at the **CUT**, this was done as shown in Equation 2.9, proportional to the mean value and constant calculated in equations 2.7 and 2.8 respectively [7].

$$T = \alpha\sigma^2 \quad (2.9)$$

The process was iterated over the whole signal, and a continuous threshold was calculated. A target was said to be detected if the signal is above the threshold [7], shown in Fig. 2.10.

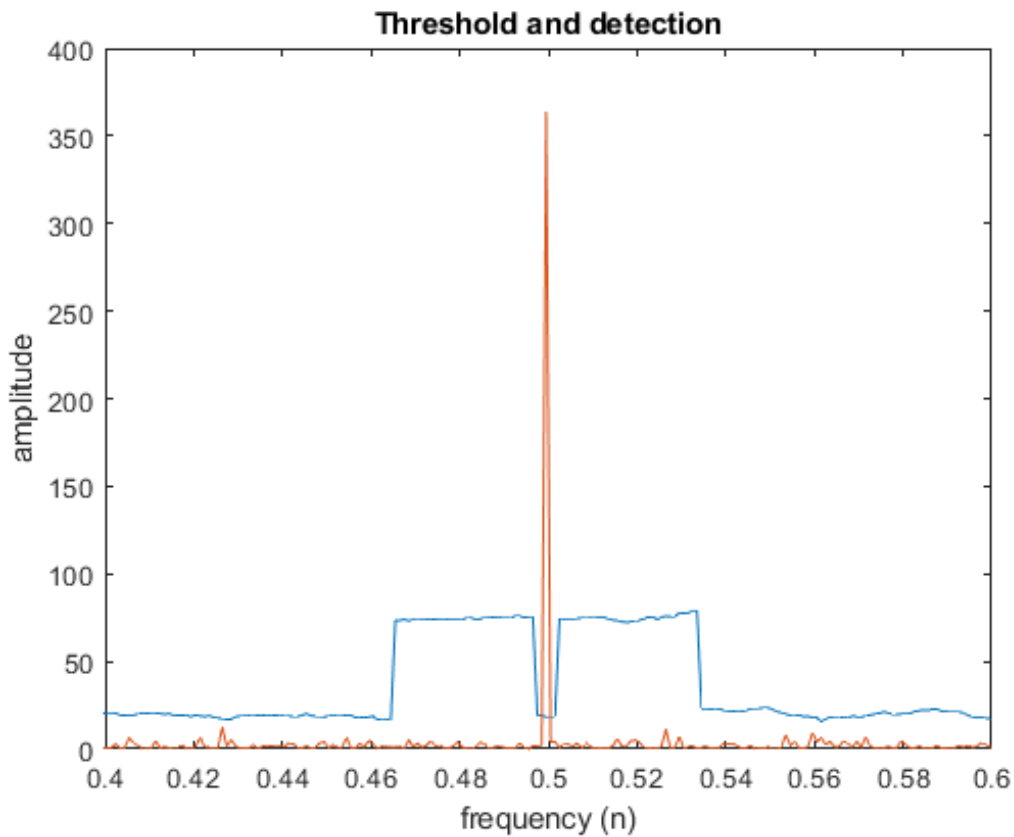


Figure 2.10: Threshold plotted against a signal with a target detected.

In Fig. 2.10 the blue line is representative of the threshold. The orange line represents the signal of the target and noise together. The x-axis has represented the Doppler frequency (could also be plotted as speed) since measurements were taken in CW and the Doppler frequency is what was intended to be measured. It is important to note that the threshold has increased as the point approaches the target (at  $n=0.5$ ), this is due to the reference window that has taken the target as a data cell when calculating the mean [7]. The threshold value noticeably drops at point  $n=0.5$ , this is due to the CUT being the cell containing the target. Hence, not part of determining the mean. It is also seen that the signal has intersected the threshold at this point, this concluding that a target has been detected.

# **Chapter 3**

## **Literature Review**

### **3.1 Traffic calming and Road Surveillance**

Traffic calming refers to the techniques used to ensure safety for pedestrians, cyclists and drivers. This is more about enforcing the rules or regulations put in place by local officials. Techniques used are often categorized by either contact or non-contact methods. These techniques target motorists by combating speeding and other unsafe practices. [15]

Whereas Road surveillance encompasses the practices of monitoring, tracking and recording the usage of roads. Road surveillance assists in road safety as it helps identify safety concerns that may arise. The methods are used to count, classify, and measure the speed of vehicles that use the road. Implementations such as magnetic loops, ultra-sonic, infrared, and camera-based sensors. [16]

Both traffic calming and road surveillance can work in tandem with each other to provide better performance in the techniques. Road surveillance can provide a means to enforce traffic calming. This could include knowing the types of vehicles on the road as to which traffic calming solutions should be implemented. Speed tracking devices, which could be used to enforce laws, could also be considered part of road

surveillance.

## 3.2 Effectiveness of traffic calming

Implementations of traffic calming by road pattern planning have been shown effective in countries such as Netherlands, Norway, France and UK [17].

One of the most common forms of traffic calming involves speed limiting. It has also been shown that speed reduction produces the greatest reduction of accidents. Compare to the 50% reduction in road injuries seen when driving at 50km/h, 90% could be avoided at speed of 30km/h, specifically in pedestrian rich areas [18].

## 3.3 Speed reduction and monitoring

Some methods used to reduce speed are meandering roads, road narrowing and traffic circles, seen in Fig. 3.1. These forcefully deflect drivers horizontally, resulting in a speed decrease. Reduction utilizing vertical deflection can also take place, this involved speed bumps, cat eyes and raised intersections. Alternatively, speed reduction can be achieved by psychological means, this would be tree planting, two-way streets, and speed monitoring [19].

Although all vehicles are equipped with a built-in speedometer, it is often overlooked by the driver. This is due to its static nature. consequently, vehicles often travel at faster speeds than what the driver is consciously aware of, especially seen in more experienced drivers. It has been shown that this lack of feedback creates a false sense of confidence in drivers. Therefore a viable solution to this would be a way to provide an alternative means of feedback to drivers on the speed at which they drive. The external and novel aspects of this will be more likely to attract the attention of the

driver, thus providing a more effective means of speed monitoring [20].



Figure 3.1: Traffic circle used to reduce speed, implemented in Addis Ababa, Ethiopia.

In Fig. 3.1 the circle directs traffic around it, this slows vehicles down. Compared to an angular turn, vehicles would gradually perform the movement, the speed reduction has shown an improvement in road safety [18].

### 3.3.1 Other methods

For certain traffic calming techniques used, there is a need for road surveillance techniques. This serves as a way to ensure that drivers adhere to the laws, or form a key part of the traffic calming technique. These are often achieved by a technical approach. They are likely to serve a single purpose. Some may include: [21]

- Magnetic loops: Detects when vehicles pass through a magnetic field, as seen in Fig. 3.2. Consequently, determine average vehicle speed, traffic light infringement and road usage [21].
- Camera detectors: Able to detect speed, quantify, and classify vehicles [21].
- LI-DAR detectors: Can be used similarly as above. Which also provides higher accuracy [21].
- GPS trackers: highly accurate and robust means of determining speed, acceleration and position [19].

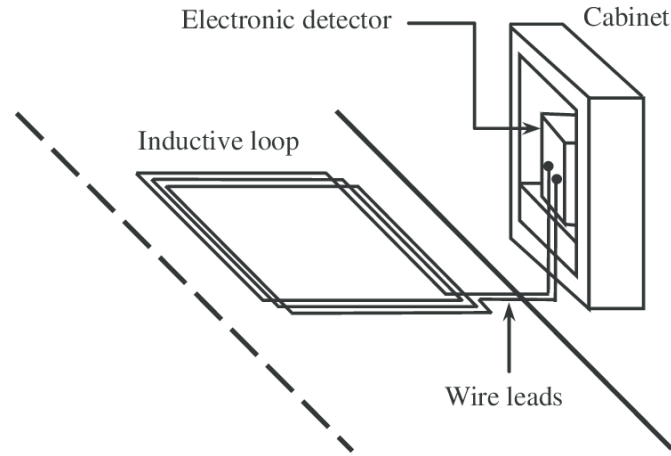


Figure 3.2: Magnetic loops used in vehicle detection [22]

All these have been shown to provide accurate and usable speed measurements. However, they also come with their caveats. Magnetic loops require construction and are costly to implement [22]. The cameras are susceptible to misreading. LI-DAR detectors are highly sensitive to weather disturbances, and often restrained by issues of alignment and range [23]. GPS trackers introduce privacy concerns, and implementation is only possible in known vehicles [19].

### 3.3.2 Radar methods

Another technique is the usage of radar in speed detection. Radar has been shown to provide levels of accuracy similar to LI-DAR detectors. When compared to laser detectors, Radar has shown to be more effective in decreasing speeds. It has been found to detect targets more often [24].

Radar also allows for a far more automated approach in speed detection. This means that limited human resources available for operation will not be a problem [24].

#### Alternative Radar Method 1

A Side-Looking Single-Radar speed detector was evaluated on estimating the speed of a moving vehicle. This device makes use of 2-D Doppler Frequency Modulated Continuous wave (FMCW) radar with a squint angle seen in Fig. 3.3. It was considered that it be installed at an angle as it allows for an enhanced Doppler frequency returned [25].

This device operates by initially determining the range. The device then sets a threshold based on this range estimation and measures the time that the target spends in the sensing region. Following this, the device performs a Doppler FFT algorithm on the signal to estimate the velocity. Consequently, the device can determine the vehicle length.

Information regarding what has determined the true vehicle speed was not provided.

---

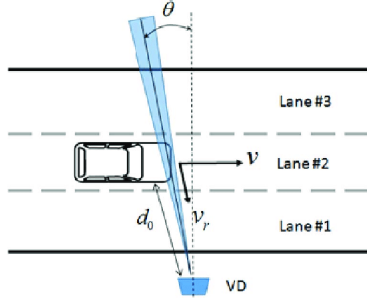


Figure 3.3: Set up of Single Side looking Radar [25]

It was concluded that the device does provide an acceptable estimation of the speed, with an error of less than 4km/h [25]. However, this was limited to speeds up to 50km/h only. Performance was observed to get worse at higher speeds [25]. This device has been shown to detect smaller targets such as bikes and pedestrians. This device is also able to accurately measure targets across multiple lanes [25].

### Alternative Radar Method 2

A three-step algorithm to estimate the ego-motion of vehicles from radar was tested [26]. These steps are as follows:

1. Outlier and non-stationary object detection. This is implemented by dropping out samples not seen to be fitting the regression line for a subset of the data. this is referred to as the RANSAC [27] method.
2. Next a velocity profile is extracted using least squares estimation.
3. Lastly, the ego-estimation is done with the Ackerman condition of the sample from step two [26].

The investigation was done to determine a method to replace the existing methods used by vehicles in providing ego-motion estimated to drivers.

The investigation was conducted based on data collected from two onboard Doppler radar sensors. The radar operated in the frequency band of  $f = 76\text{GHz}$  [26].

Speed measurements had shown an average accuracy of 0.36km/h. It was concluded that this method could replace the odometry methods currently used on vehicles. However, this is heavily dependent on the radar sensor parameters [26]. Furthermore, this algorithm may not always be considered effective as a bias exists from the least-squares method.

### Commercial solution

Radarsign has made a speed detection radar available commercially [3]. The radar operates in the K-band, as pulse-doppler. The radar makes use of a centre frequency of 24.125GHz. It is able to detect targets 365m away, of speeds between 8-200km/h. On the product page it is said that a speed accuracy of 1.6km/h [3]. The speed is displayed to the driver as seen in Fig. 3.4.



Figure 3.4: TC-400 radar display by RadarSign [3].

### 3.4 Proposed method

This thesis exists as a continuation of the investigation conducted in [6].

Investigation into using a mobile S-band radar for traffic calming applications was done. The radar used was adapted on plans provided by the MIT IAP Radar Course. The transmitted radar signal had a centre frequency of 2.45GHz. The method consisted of the detection of a moving target in recorded radar data. Consecutively, speed was extracted using the detected Doppler frequency of the target. Measurements were taken on multiple vehicles driving at varying speeds. True speed data

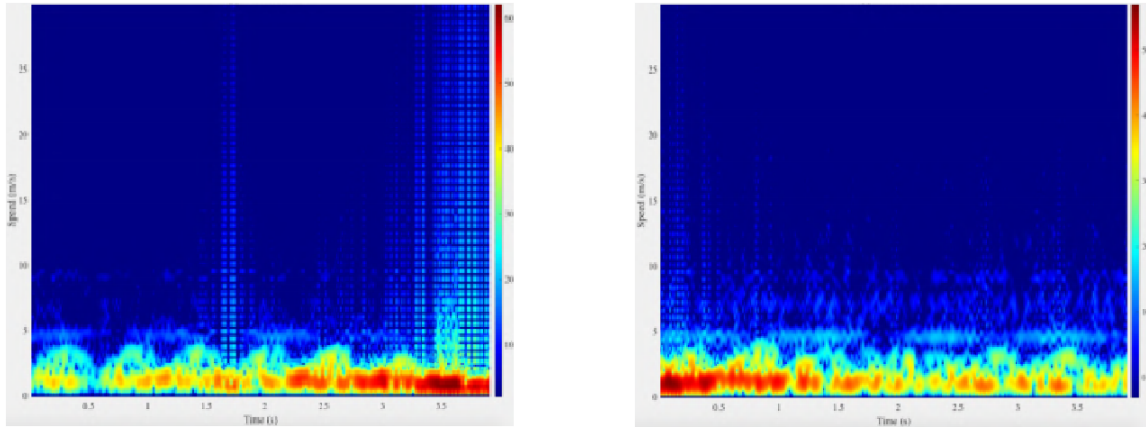
was taken from the on board speedometer readings.

The investigation process has been summarised as:

1. Construction and testing of MIT S-band radar.
2. Simulation of target detection algorithms.
3. Measuring radar data used in the investigation.
4. Processing measured by performing the **STFT**.
5. Employing the target detection algorithms simulated.
6. Extracting speed estimated based on the detection algorithms used.
7. Comparison of various **CFAR** processes and performance.
8. Evaluation of performance against true speed values.

### 3.4.1 Radar Testing

Radar testing was done to ensure that the radar was performing as specified. Testing was done in **CW** and **FMCW** modes. Results seen in **CW** mode were displayed on the spectrograms shown in Fig. 3.5.



(a) Spectrogram generated from radar data of person walking towards the radar

(b) Spectrogram generated from radar data of person walking away from the radar

Figure 3.5: The results of testing the constructed radar [6]

Fig. 3.5 shows that the radar was operating as expected. The speed extracted from both walking towards (Fig. 3.5a) and walking away (Fig. 3.5b) was seen to be 15km/h, this matches the average walking speed of a human. Both measurements seen in Fig. 3.5 display noise, however, this was expected due to environmental conditions.

### 3.4.2 Target Detection

Furthermore, a comparison of various CFAR techniques was done. Ordered Statistic-CFAR (OS-CFAR), Ordered Statistic Greatest Of-CFAR (OSGO-CFAR) and, Cell Averaging-Constant False Alarm Rate (CA-CFAR) were the techniques investigated. Findings were recorded and summarized in Table. 3.1.

	Processing Technique		
	OS-CFAR	OSGO-CFAR	CA-CFAR
Single Target Detection	Entire	Entire	Partial
Multi-Target Detection	Both	Both	Single
Clutter Boundary	No False Alarms	No False Alarms	False Alarms
Speed estimation (exp. 45km/h)	44.7 km/h	44.7km/h	44.7km/h

Table 3.1: Comparison of CFAR techniques [6]

As seen in Table 3.1 all three of the techniques discussed have been shown to produce the same speed. this is due to all techniques making use of the same clustering algorithm.

Differences in multi-target detection, false alarms and target detection have also been shown. It was also stated that OS-CFAR has produced the most detection overall and OSGO-CFAR the least [6], justified by the OSGO-CFAR with the most rigorous technique of minimizing false alarms. Worse overall performance was seen with the CA-CFAR, specifically in multi-target detection and false alarm rates [6]. It was decided that further investigation was to be done using the OS-CFAR technique of target detection.

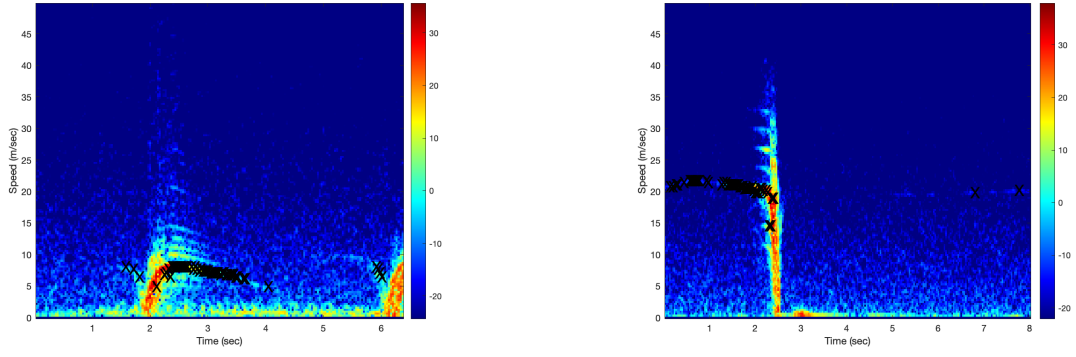
### 3.4.3 Results

Radar performance was assessed based on the following criteria [6]:

- Speed estimation accuracy compared to the speedometer and GPS reading.
- Detection of the vehicle when approaching and departing from the radar.
- Speed detection of different vehicle sizes.

- Detection in different environmental conditions.
- Detection of multiple vehicles, and determining the speed of the maximum vehicle.

Some generated spectrograms can be seen in Fig. 3.6.



(a) Spectrogram generated from a bike travelling at 30km/h

(b) Spectrogram generated from SUV travelling at approximately 90km/h

Figure 3.6: Generated spectrogram between cases of smallest and biggest ROC measured [6]

In Fig. 3.6 locations of detected targets are marked with 'X'. Fig. 3.6a some false alarms were detected near the bottom right. Fig. 3.6b false alarms were also detected closer to the middle of the displayed speeds. Speed was shown in m/s and subsequently converted to km/h before the comparison was made. The speed estimations seen were accurate in Fig. 3.6a. Alternatively, a noticeable difference in speed was found in 3.6b, where the measured speed of 78.31km/h was found when the expected speed of 90km/h was expected [6].

Results from all data sets tested were summarised in Fig. 3.7. The Test events axis represents each data set used. The speed from each dataset is represented on the y-axis, where blue represents the speedometer, orange the GPS and grey the

measured values. It was observed that the error increases as the speed increases, starting at a value of 4.9% at 20km/h to an error of 15.67% at speeds greater than 120km/h [6].

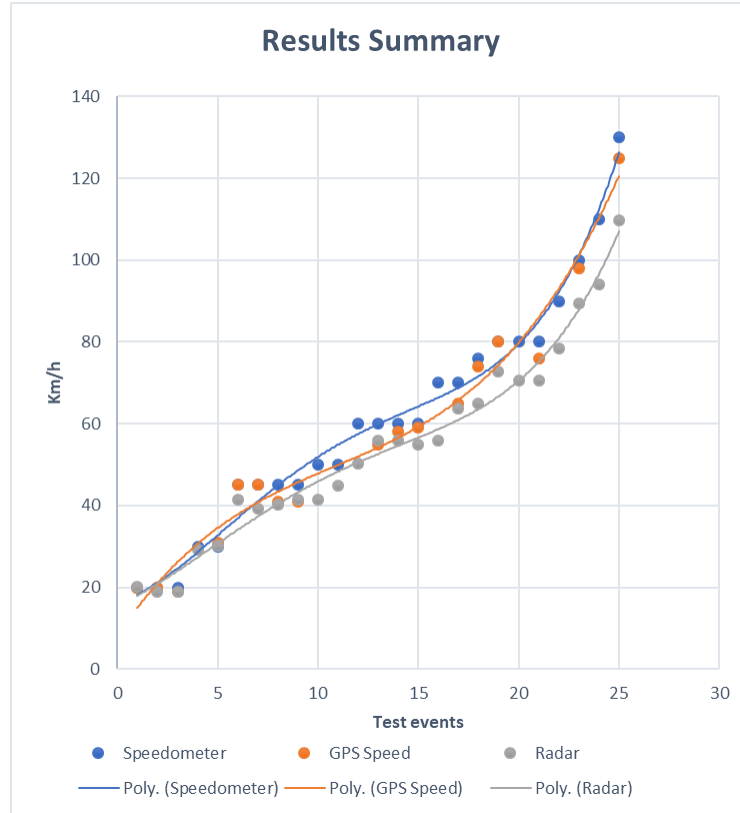


Figure 3.7: Summaries results from the experiments performed [6]

Overall it was decided the performance has met the specified criteria, thus performing adequately. Furthermore, it was found that the accuracy of detection was proportional to the RCS and inversely proportional to the speed of the target. An average error of 9.9% was found [6].

### 3.4.4 Work Omitted

After comparison was done between the CFAR processes, no further work was done on CFAR processes that were not OSGO-CFAR. The effect of CFAR input parameters on performance was not investigated, specifically in CA-CFAR. Furthermore, the effects of varying input parameters values in the STFT were not investigated.

# Chapter 4

## Methodology

### 4.1 Approach

In this thesis, data measured from a CW radar has been used. The CA-CFAR method was used for target detection.

Investigations were conducted to determine optimum parameter values. Effects of varying parameters were also investigated.

Initial verification was done on the algorithms used. This was conducted on simulated data, with predictable results.

### 4.2 Literature and Theory

A literature review was conducted. It involved research into existing research in the field of traffic calming. Further investigation was conducted on techniques used to detect speed. Research on target detection techniques in radar data has also been done. Part of the investigation was a critical analysis of short-fall within the various proposed solutions. This also assisted in the development of further understanding of the problems and unaddressed issues faced.

The theory behind the experimental procedure was conducted. This provided an understanding of how to properly implement algorithms used. This also assisted in determining which parameters to investigate.

### 4.3 Simulation

Initial testing on simulated data was done to assess the performance algorithm implemented. This was done as explained below.

Simulated digital sinusoidal signal data was generated. These were generated as both real and complex, done directly or by the addition of two signals. The **FFT** function was used and the spectrum was analysed as validation.

Using the methods as tested above, a chirp signal, of known parameters, was generated. The code that was made to generate the spectrogram was used with the chirp as input. The spectrogram was then assessed based on the known parameters and a comparison was made with the built-in MATLAB function.

The processing steps required to implement the **CA-CFAR** algorithm was coded with functionality to easily change parameters. Gaussian noise was generated, and plotted on the spectrogram. The **CA-CFAR** algorithm was then applied with a known **PFA** and the PFA-error was assessed to ensure sufficient operation. A method to plot detected target location was also implemented, and evaluated by sight.

Generated target signal was added to the noise. The target location algorithm was applied again to provide an extra means of validation.

### 4.4 Experimental procedure

A brief outline of the method followed in conducting the investigation.

#### 4.4.1 Procedure

##### Procuring Data

The data sets used in evaluation and testing was measured by a final year student, Ms Najaar in 2019 [6] this is shown in Fig. 4.1. This was sourced using the S-band radar design that was adapted from plans provided by the MIT IAP radar course.

Some specifications of the radar and data are as follows:

- Bandwidth: 80MHz.
- Centre frequency: 2.45GHz.
- [Continuous wave](#) mode.
- Data measured in a heterogeneous environment.
- Constant velocity of target within radar range.
- Sample rate of data: 44100Hz
- Multiple vehicle models used [6]

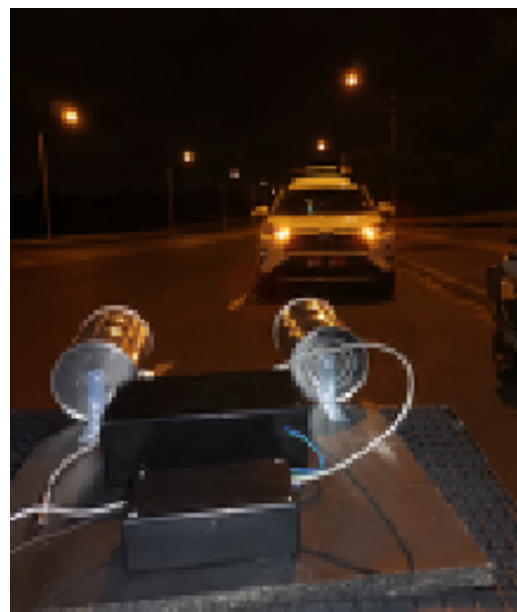


Figure 4.1: The completed radar used to measure data, provided by [6]

Radar measurements were taken based at an unspecified aspect angle. Thus, the speeds derived would be that of the radial velocity. Linear speed was therefore approximated at the maximum speed detected, as it would provide the minimum angle. In measurements taken adjacently, shown in Fig. 4.2a, there was an increase with the velocity with respect to time, resulting from the change in aspect angle. Directly perpendicular measurements, as shown in Fig. 4.2b provided a constant frequency and speed reading, due to a constant angle.



(a) measurement taken at an angle to the movement



(b) measurement taken perpendicular to movement.

Figure 4.2: The experimental setup used when measuring data

Each data set has been evaluated individually. Initially loaded into MATLAB as a '.wav' file, and subsequently was prepared for processing.

### STFT and Spectrogram

Parameters shown in Table 4.1 were set to specified values. Data was subsequently sent to the STFT, and the spectrogram was generated using the same algorithm that was verified in the simulations. Observation and evaluation were done to confirm hypotheses on the effects of altering the variables.

Frequency data were converted to speed and limited to the display over a reasonable interval.

### Cell Averaging-Constant False Alarm Rate

The CA-CFAR algorithm was then implemented. Parameters shown in Table 4.2 were set. Locations on targets found in the displayed interval were marked out on the spectrogram. Evaluation of performance was done on the false alarms and missed targets. Exploration of the effects of alterations of these variables was also done.

### Determining Speed

To plot speed, the mean value of targets found per window was plotted against time. This was taken as the final reading where a single value was approximated from time. Further evaluation was done on the results. However, results shown in this stage yield very similar to previous stages. The Speed vs. Time plot was done mainly to display data more intuitively.

### Parameter Optimization

Parameter values were set manually within MATLAB. Based on theoretical knowledge the assumed parameters to vary were chosen as well as decisions on how.

Parameters chosen are shown in tables 4.1 and 4.2 below:

#### 4.4.2 Validation

##### Ground Truth

Recorded data were labelled according to speed. Readings taken from an on board speedometer was used as true speed values.

Table 4.1: Input parameters varied in STFT and Spectrogram

Parameter	Function and Effect
CPI	Coherent Processing Interval, determines the number of samples within each window frame. Physically represents the duration of the data that each window performs the FFT on in the STFT process. Varies the frequency and time resolution.
OLF	The amount of overlap between each consecutive frame in the STFT. Will physically affect the time taken between each sample of the STFT. Impacts the time resolution.
Window Function	The windowing function used in the STFT. This affects the magnitude of the signal before the STFT. This would then influences the signal power after the STFT.

Table 4.2: Input parameters varied in CA-CFAR

Parameter	Function and Effect
PFA	Desired probability of false alarm. Used in computing the threshold in the CA-CFAR process. Refers to the desired probability of a target being detected within a noise-only signal.
RefWindow	The number of data cells to be used on either side of the CUT in the CA-CFAR. Will affect the threshold value and is limited by the frame length.
gcell	The number of guard cells to use on either side of the CUT.

## Validation

Speed measurements from the Final speed vs Time plot were used to approximate a speed at a specific time instance for each reading. A comparison was made to the known speed value, subsequently, evaluation was done based on accuracy and detection rates. Further observations were made on non-conforming data.

### 4.4.3 Process Summary

A summary of the process described above is summarised in Fig. 4.3

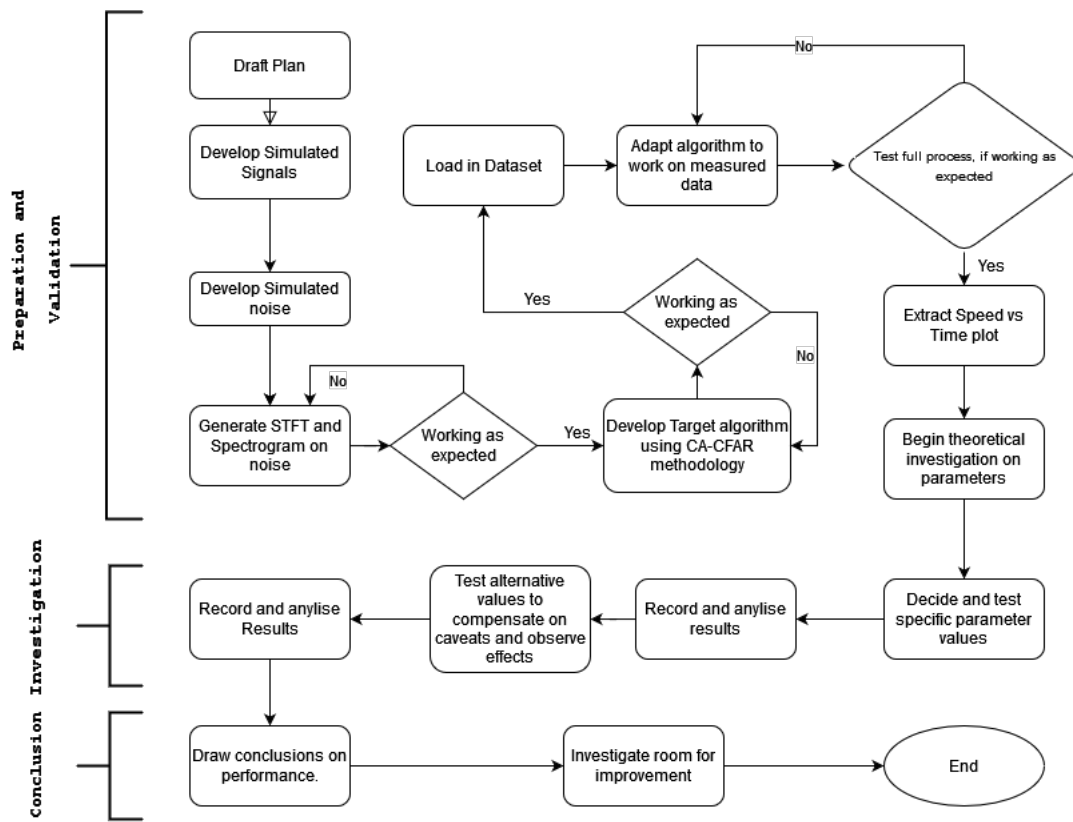


Figure 4.3: Summary of the methodology used to develop and execute the investigation.

# Chapter 5

# Design

This section has covered the methods used to Validate, Implement and perform the investigation. The way that the theory covered in Chapter:[2](#) has been implemented in the methodology that was briefly explained in Chapter:[4](#) has been explained in this chapter.

## 5.1 Validation

To ensure experimental validity, the implemented algorithms were tested on simulated data. As described in chapter:[4](#) validation was performed when generating sample data, the spectrogram and on the [CA-CFAR](#) algorithm.

Initially, a variety of signals were produced, each with defined specifications, plotting of these signals were done as validation (Appendix a).

In the simulated spectrogram, a target signal was added to Gaussian noise of specific sample length (Appendix A). This signal was inserted midway through the noise signal. Other parameters such as the SNR was also specified. Validation for this was done by plotting the signal at an arbitrary time length, this is seen in Fig. [2.10](#).

A 1-second chirp signal was used to validate the algorithm used to develop the spectrogram (code in Appendix A). The chirp signal was generated with a start frequency of 20Hz and an end frequency of 40 Hz. the spectrogram was then generated. Parameters of the STFT were changed, and results were observed and compared to theoretical estimations. The comparison was made to the MATLAB built-in spectrogram function.

First validation of the CA-CFAR was performed on purely Gaussian noise (Appendix A). A specified PFA of  $PFA = 1e^{-3}$ , and with a set length length of 100000 samples. Equation 5.1 was used to evaluate the PFA-error ( $PFA_{err}$ ) based on the actual PFA of the CA-CFAR ( $PFA_{sim}$ ), the simulation was regarded as valid if  $PFA_{err} < 10\%$ .

$$PFA_{err} = \frac{PFA - PFA_{sim}}{PFA} \times 100 \quad (5.1)$$

The last step of validation used was in marking the locations on the spectrogram, the target+noise signal used, and partly displayed in Fig. 2.10 was used to generate the spectrogram. Subsequently, target locations were marked and verified as correct by sight (Appendix A).

## 5.2 Implementation

### 5.2.1 Short Time Fourier

The algorithms that were validated as shown in Chapter: 5.1 were adapted to be implemented on measured data.

Initially each data-set was loaded in individually. Data was initially loaded in from a two-channel .wav file format (X) with the sampling frequency (fs) . The code shown in listing 5.1 shows how the data was initially loaded in and converted to a single channel input vector (x), 'fname' is the file name of the data-set being tested.

Listing 5.1: Code used to prepare data

```
[X, fs]=audioread(fname , 'native ' );
x = -X(:, 2);
```

The Parameters chosen in Tables: 4.1 and 4.2 were set as shown in lines 2-7 of listing 5.2. Line 9 has called the function that performs the STFT which called the CA-CFAR and speed detection algorithms.

Listing 5.2: Input Parameters being set

```
2 fname = 'Audi_A1_Driving_Away_30KPH.wav';
3 CPI=0.8;
4 OLF =0.5;
5
6 pfa = 10^-14;%desired Probability of false alarm
7 RefWindow =500;%size of data cells
8 gcell=2;% number of guardcells
9 MakeX(fname ,CPI,OLF,pfa ,RefWindow , gcell)
```

The STFT was applied to the data in lines: 42-48 (code provided in Appendix A). This was done by applying the window function, performing the FFT on the input signal, from which the DC component was removed. This was iterated at each window position and saved as an NxM matrix (N=number of frames (factor of time), M=frame length (factor of frequency)). In lines: 51-52 the time and frequency axes were defined with respect to the samples per frame (Ns), sample frequency (fs) and

hop (slide).

As seen in listing. 5.3, the Window Function type was defined at line 38. Line 34 calculated the window length as a number of samples (Ns), it was ensured that this is a power of two, for purposes of the DTFT which is outside the scope of this report. A new value of CPI was calculated to account for the rounding that takes place in computing the frame length. The hop was calculated at line 36, based on the OLF and Ns. Followed by the number of frames, proportional to the length of the signal.

Listing 5.3: Window function preparation

```

33 %Preparing the window
34 Ns=2^nextpow2(CPI*fs) ;
35 CPI=Ns/fs ;
36 slide= floor(Ns*(1-OLF)) ;
37 Nf=floor(((N-Ns)/slide)+1);
38 win = hamming(Ns);%not sure how i would go about changing
    the type outside the function

```

Post STFT signal data was plotted initially plotted with respect to frequency in the validation phase. To convert this to speed as shown in Equation 2.3 was used, and subsequently converted to km/h, the algorithm shown in lines: 55-57 in listing 5.4 was applied. The frequency range of the antenna provides the ability to track speeds higher than what is needed for this implementation, hence, 'SpeedVectorOfInterest', 'speed\_km\_per\_hr\_Idx' and, 'S\_OfInterest' was defined, limiting the display to plot speeds from 0-100km/h.

Subsequently, the spectrogram was plotted as a function of Time vs. Speed vs. Power (dB).

Listing 5.4: Doppler frequency to Speed (km/h) where 'c' is the speed of light.

```

55 lambda = c/fc ;
56 speed_m_per_sec = fax*lambda/2;
57 speed_km_per_hr = speed_m_per_sec*(60*60/1000);
58 speed_km_per_hr_Idx = find((speed_km_per_hr <= Maxspeed) & (
59   speed_km_per_hr >= 0));
60 SpeedVectorOfInterest = speed_km_per_hr(speed_km_per_hr_Idx)
61   ;
61 S_OfInterest = stfft(speed_km_per_hr_Idx, :);

```

### 5.2.2 Target Detection

Based of the parameters chosen, the CA-CFAR algorithm was applied (lines 82-85 and 111-136, code provided in Appendix A). This iterated through each time step and applied the CA-CFAR method on the signal through the frequency axis. The function 'CACFAR' returned an array of target indices with respect to the whole signal. Which was used later when detection was marked on the spectrogram.

The input signal was passed through a square-law detector and the value for  $\alpha$  was calculated (Equation 2.8) on line 119. The threshold was calculated per Equation 2.9, which iterated across the whole signal (at time step). The CUT (Fig. 2.7) was taken from the 'speed\_km\_per\_hr\_Idx' (which corresponded to the indexes of the signal of the range of speed interested in). However, data cells were able to be indexed outside of this vector. The CUT was incremented by 1 at each iteration. The mean value ( $\sigma^2$ ) was calculated and the threshold ('thold') was evaluated for the CUT.

Detection algorithm has also been implemented (lines 130-133, Appendix A) at each CUT. The index, with respect to the 'speed\_km\_per\_hr\_Idx', was recorded if a detection was found. This was done for each time iteration and stored in a matrix.

### 5.2.3 Speed Detection

After CA-CFAR processing, the targets detected ('detect') were plotted as 'X' markers on the spectrogram. The purpose of this investigation was to minimise errors in this detection.

Speed data was displayed as a function of Speed vs Time. This was done by calculating the mean speed of detections over each time instance (Lines: 108 and 138-147, Appendix A), converting into a 2-d matrix. Subsequently, this was plotted as a line graph. The approximation of speed detected was made as the max value displayed on the graph.

## 5.3 Experimentation

Parameter values chosen were initially researched. Trail-and-error was not the main factor in determining these values, however, some iterations had to take place to correctly assess the optimum performance. The results were evaluated on the ability to detect targets, minimise false alarms and, provide an accurate speed estimation. It was also assessed on data sets containing targets both, departing and arriving. Although multi-Target data sets were tested, it was not expected to be part of the main criteria, and was just a means to evaluate improvements on results seen in [6].

### 5.3.1 Considerations

Important general considerations were made when determining the parameters. These were not specific to a single parameter but still impacted the decisions made. The considerations made were as follows:

- Radar Power vs aspect angle: Due to radial velocity measurements, and the

radar equation (Equation 2.2) the power seen at the minimum aspect angle would have a lower detected power when a vehicle is driving past the radar, as this will occur at the furthest distance away.

- Maximum Expected speed: Based on the nature of the expected targets, estimations were made on the range of speed. It was expected that the radar system was to be implemented in small residential areas, therefore further maximum speed estimation can take place. Measured data was on known speeds. These factors mentioned resulted in a decision of the maximum speed of 100km/h to be expected. Limiting the range of speeds to take readings from has lessened the effects of interference, specifically of fast-moving objects near the sensor.
- The target RCS was considered. Since detection was required for a range of vehicle sizes, and at varying distances, the RCS would vary between data sets.
- Other aspects were also considered. However, specific to this use case it was deemed as not as impactful on the performance.

### 5.3.2 Coherent Processing Interval

The CPI has determined the frame length and affected both the temporal and frequency resolutions of the data. Equation 5.2 converts the CPI to a frame length (Ns), based on the sampling frequency (fs).

$$Ns = fs \times CPI \quad (5.2)$$

A higher CPI value provided a better frequency resolution. Based on the data and methodology used, it was decided that a higher frequency resolution would be favoured. A higher frequency resolution lessened the number of detections per

target per time step. This was shown as a more accurate reading as the doppler frequency was determined more precisely. Temporal resolution was also decided to be of lesser importance compared to the frequency since the maximum value of speed was approximated from only a single time step, and the change in velocity with respect to time was of lesser importance to meet objectives, also some cases it is seen as generally low importance. CA-CFAR processing was done with to the frequency axis, hence a higher frequency resolution would assist in target detection. A higher frequency resolution also allows smaller targets with a smaller RCS to be detected more frequently providing better estimates.

However, employing too high of a CPI was shown to be too taxing on the hardware used to provide accurate testing. It was also noted that the low temporal resolution had a chance of not displaying the actual maximum speed resulting in less accurate readings.

### 5.3.3 Overlap Factor

A higher value for the OLF has been shown to compensate for temporal losses. However, this has been shown to possibly come at higher computational costs. Too much overlap also resulted in higher frequency amplification. However, the limiting of the range of frequencies interested in has been limited, and higher frequencies have been neglected when detecting targets. In Fig. 5.1 It has been found that the optimal value to set the OLF to is 50% [14].

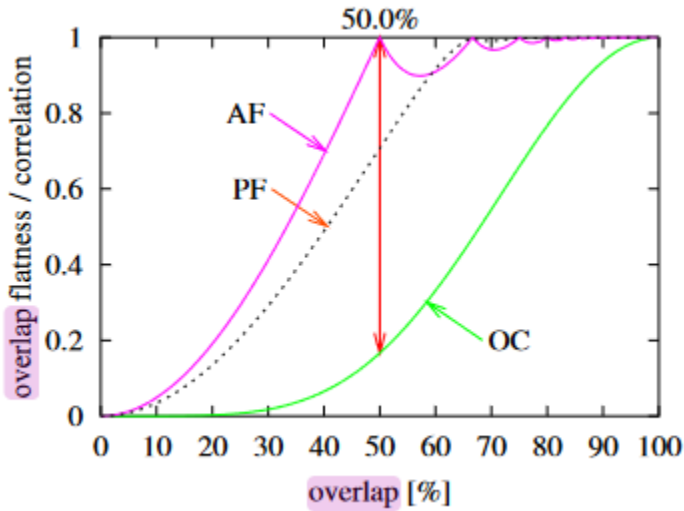


Figure 5.1: The performance of a Hanning window with regards to the % overlap [14]

In Fig. 5.1 it is shown the % overlap vs overlap flatness. The overlap flatness is an assessment of the the weighting that each data point in the signal receives due to the window applied. The blue line refers to the amplitude flatness (AF). This is measured after the window has been applied to the whole signal. The metric used evaluates ratio between lowest weighted discrete impulse to the highest. A value of 1 signifies that all samples were of equal weighting, the window applied effected each discrete data point the same. This is desired when all points are considered of equal importance. Power flatness (PF) has a similar meaning to that of AF, however, PF sums the weighting of the signal quadratically, this considers the impact of noise. a higher value is often desired. Overlap Coefficient is metric of correlation between the spectrum estimates of subsequent stretches. It also serves as a measurement of computational effort [14].

### 5.3.4 Window Shape

When choosing a window there is a trade-off between bandwidth and side lobe gain, decreasing the side-lobe would increase the bandwidth [14]. It was desired that both be minimized as possible. The Hanning window has shown a -88dB attenuation in the side lobes, and a -3dB Bandwidth of 1.2 bins, bins refer to the space between each frequency sample in the discrete samples. This was chosen as a well-suited middle ground which can be seen in Fig. 2.6b.

### 5.3.5 Probability of False Alarm

The **Probability of False Alarm** was taken based on how high the desired threshold would be considering the data. The **PFA** value has taken both the frequency and temporal resolution into account, as this would provide the number of samples tested, thus the number of false alarms.

Ideally, a **PFA** of 0 was desired, however, this would be unattainable, so a low value was chosen. An optimum **PFA** would account for the SNR which was unknown in this investigation. The **PDF** of the **PFA** distribution is seen to be Gaussian. The **PDF** of the probability of detection ( $P_D$ ) is also shown as a Gaussian, the offset between the two distributions is proportional to the SNR. The X-axis represents the threshold magnitude, thus a **PFA** needs to be decided that will find the threshold minimizing the area on the **PDF** of **PFA** while maximizing the  $P_D$ . This is seen in Fig. 2.8, displaying the relationship of an arbitrary signal, noise and threshold.

### 5.3.6 Reference window

Increasing the size of a reference window would provide a more accurate estimation of the mean. Alternatively, too wide of a window would be taxing on the hardware.

Increased window width has been shown to also increase the rate of false alarms. Interference or noise was generally seen as clusters, often displayed over multiple frequencies. Thus, increasing the width resulted in the reference window taking in cells without interference. Therefore, lowering the mean. Compared to a smaller window where the reference window has a greater ratio of the higher-interference to the general interference, resulting in a higher threshold and fewer false alarm detections.

When deciding on the length of the reference window the span of the target in the frequency domain was also looked at, this was proportional to the **RCS** and inversely proportional to the distance. The decision on reference window size was made to be bigger than the targets frequency span while also being small enough to accurately determine the mean in interference. However, the threshold is also reliant on the **PFA**, so increasing the **PFA** allowed for more freedom in determining the reference window size.

### 5.3.7 Guard cells

The choice of guard cells is dependent on the frequency resolution. Factors of the Target cross-section also assist in determining the number of guard cells. The easiest method to determine an optimal value for the guard cells is to look at the spectrogram. The target is normally seen to span over 3 frequency bins closer to the point of interest.

### 5.3.8 Parameter choices summary

The values chosen for the parameters shown in Tables. [4.1](#) and [4.2](#) were summarised in Table. [5.1](#) as:

Parameter	Choice	Choice 2
CPI	0.6	0.8
OLF	0.5	
Window Shape	Hanning	
PFA	$10^{-14}$	$10^{-50}$
Reference Window	50	300
Guard cells	3	

Table 5.1: Chosen parameter values that were used

### 5.3.9 Evaluation

The performance was rated on the following criteria:

- Detection of targets
- Minimizing false alarms
- Speed estimation accuracy of a single-target
- Performance of both arriving targets and departing targets
- Performance on different vehicle sizes

When analysing results, attention was payed to each criteria separately. This was done to account for errors specific to one area, such bad reading or data conversions what would propagate as an off-set in the axis. This would then allow target detection and false alarm minimization to still be accurately assessed. When conclusions were made, attention was payed to patterns across all data sets, this also served as a method to ensure that the algorithms performed consistently.

# Chapter 6

## Results

### 6.1 Validation

The results achieved of the validation of the algorithms that were implemented are shown.

Example of generated data used as verification can be seen in Fig. 6.1. The plot displayed that the signal was generated as expected. The signal generated was of a sine wave with a period of 250ms, this is matched by the plots seen in Fig. 6.1

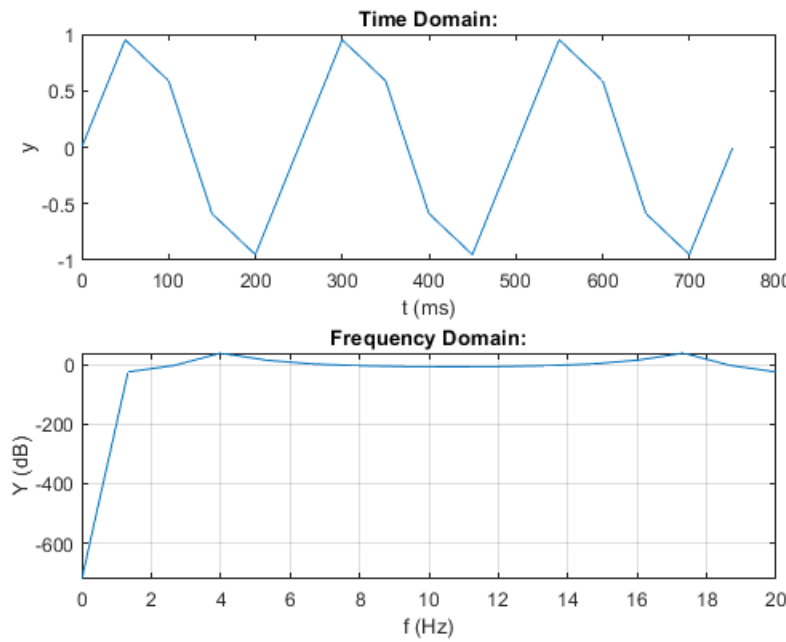


Figure 6.1: Example of generated Data

The chirp signal shown in Fig. 6.2 shows that a signal moved from a frequency of 20Hz to that of 40Hz, over the span of one second. This is in accordance to what was specified. A line of higher power is observed in the spectrogram transitioning from 20Hz to 40Hz. The background is also seen to be clear.

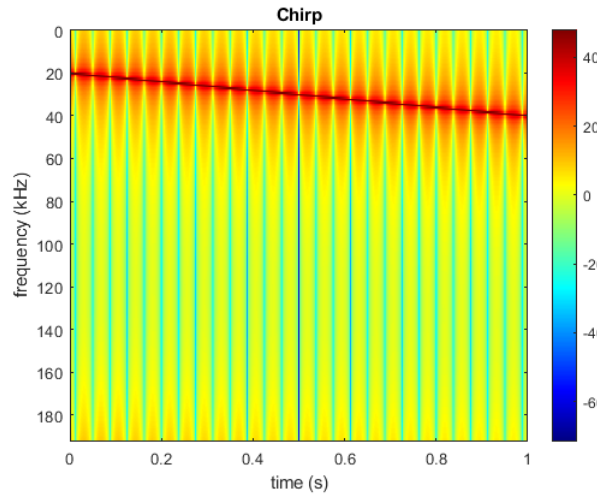


Figure 6.2: Generated Chirp signal used to test the spectrogram algorithm

When the code provided in Appendix A, was applied the PFA-error was shown to be at an average of less than 6%.

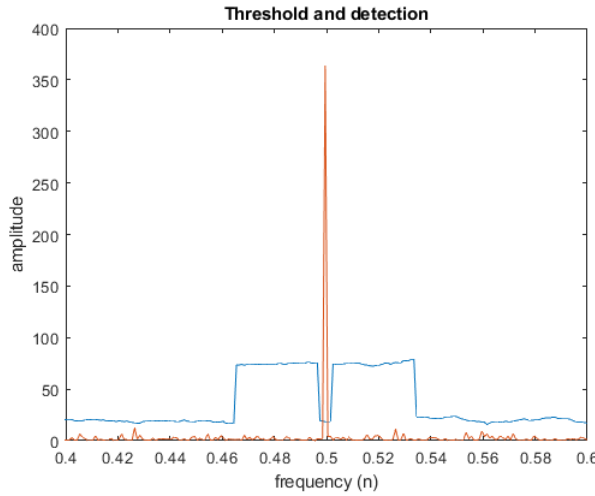


Figure 6.3: Target Detected in Simulated noise+target

Displayed in Fig. 6.3 it can be seen that the target is in fact located at the specified location. Fig. 6.4 showed that the target placed midway in the signal was

detected.

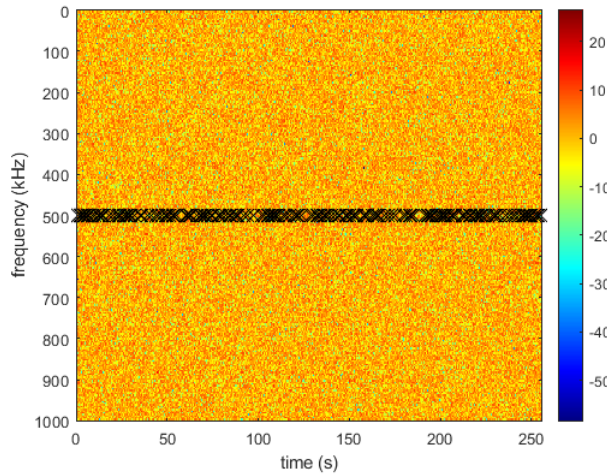


Figure 6.4: Target location marked in simulated signal of target in noise

## 6.2 Experimentation

In the experiment conducted, parameters were set to those that were chosen and tested. For instances where second values were needed, only that parameter was changed, all other parameters were set to the values shown in Table. 5.1. These were all tested on the Audi A1 driving away from the radar at 30km/h, shown in Fig. 6.5.



Figure 6.5: The set up of the radar and Audi a1 used in capturing the data used in comparisons.

### 6.2.1 Coherent Processing Interval

The first parameter that was investigated was the **CPI**. The value chosen was 0.6. The value of 0.8 was also used as a means of investigation. In Fig. 6.6 the output between the chosen value and a higher value of **CPI** is shown, for the Audi A1 driving away from the radar at 30km/h.

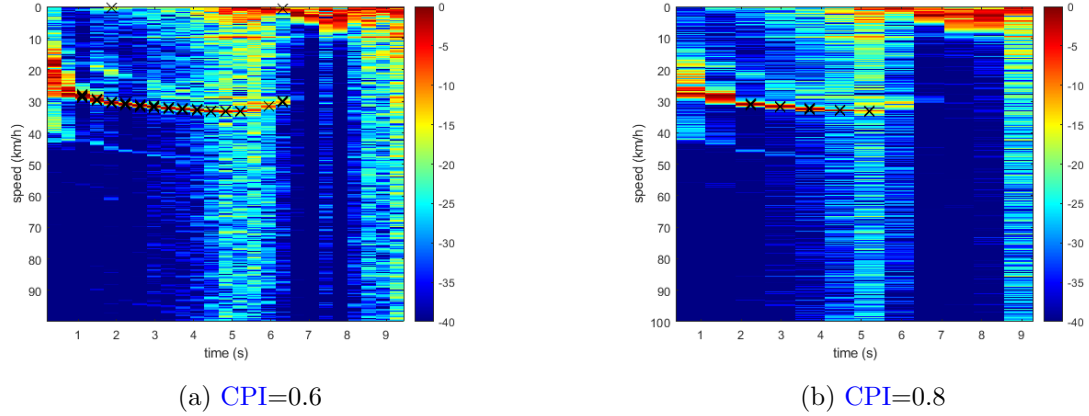


Figure 6.6: The difference of targets detected for the Audi A1 driving away at 30km/h of CPI=0.6 vs. CPI=0.8

In Fig. 6.6a it can be seen that there are more targets detected compared to Fig. 6.6b. Sparsity between consecutive targets seen in Fig. 6.6b can be seen to be wider than Fig. 6.6a, which was what was expected.

As per Fig. 6.6 and all other consecutively shown spectrograms; time is represented on the x-axis, speed on the y-axis and the colour-bar is representative of power intensity. Locations, where targets were detected, are marked with an 'X'.

### 6.2.2 Probability of False Alarm

The Probability of false alarm was another variable where two values were considered. In 6.7 the difference of detection of the PFA values of  $10^{-14}$  and  $10^{-50}$  were shown. Although, noticeably less false alarms were detected there is also less of the target detected. This occurs near maximum values of detection, hence considered undesirable.

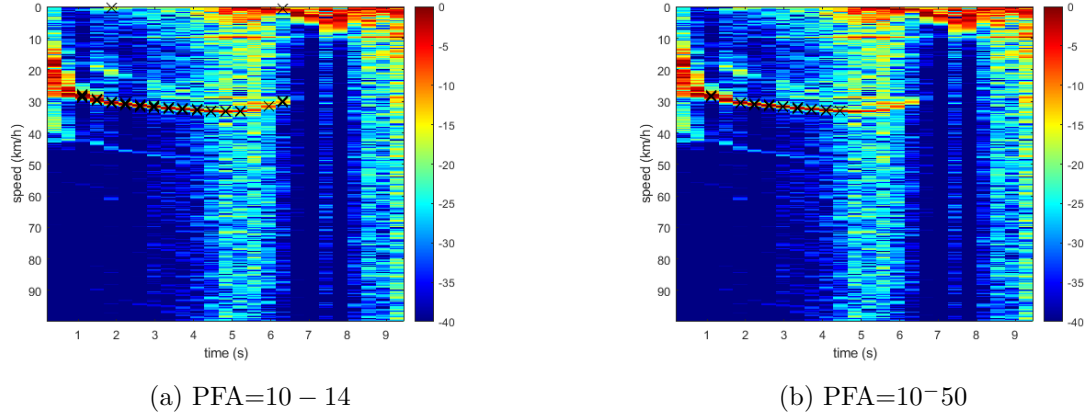


Figure 6.7: The difference of targets detected for the Audi A1 driving away at 30km/h of  $PFA = 10^{-14}$  vs.  $PFA = 10^{-50}$

### 6.2.3 Reference Window

In Fig. 6.8 the result of the experiment is shown when the Reference window length was set to 300 samples on each side. Compared to what was shown in Fig. 6.7a, it can be seen that there is a higher number of false alarms detected. This is expected as the longer window length could have reasonably lowered the mean calculated over the cluster seen at the top right in Fig. 6.8 and Fig. 6.7a. This is due to the ratio of cells with the interference to that of just the normally measured noise being lessened when a longer reference window length was introduced.

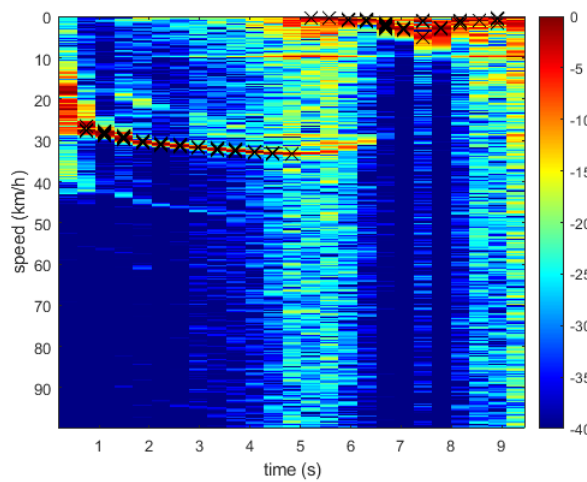


Figure 6.8: The result found when the size of each reference window was set to 300.

### 6.3 Decided parameter value

The values chosen for each parameter was set as shown in Table. 6.1.

Parameter	Choice
CPI	0.6
Overlap Factor	0.5
Window Shape	Hanning
PFA	$10^{-14}$
Reference Window	50
Guard cells	3

Table 6.1: Chosen parameter values that were used

Tests were then run on the data available.

### 6.3.1 Audi

The most consistent performance was shown with the Audi A1. The shape of the vehicle is referred to as a sedan.

Speed approximations taken from Fig. 6.9 were displayed in Table. 6.2

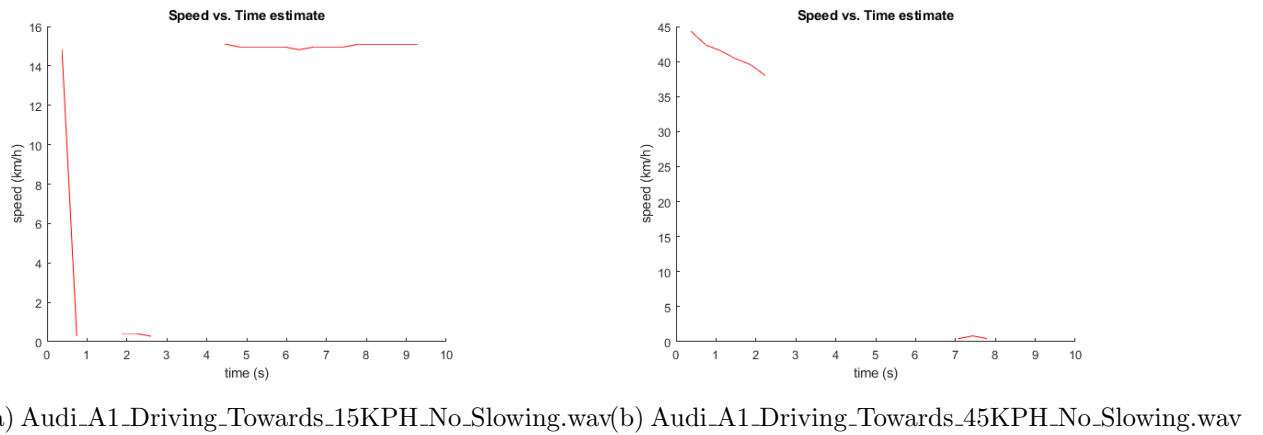


Figure 6.9: Final speed vs time plots derived from the applied algorithm on the Audi A1

Fig.	Detected Speed	True Speed
6.9a	15km/h	15km/h
6.9b	44km/h	45km/h

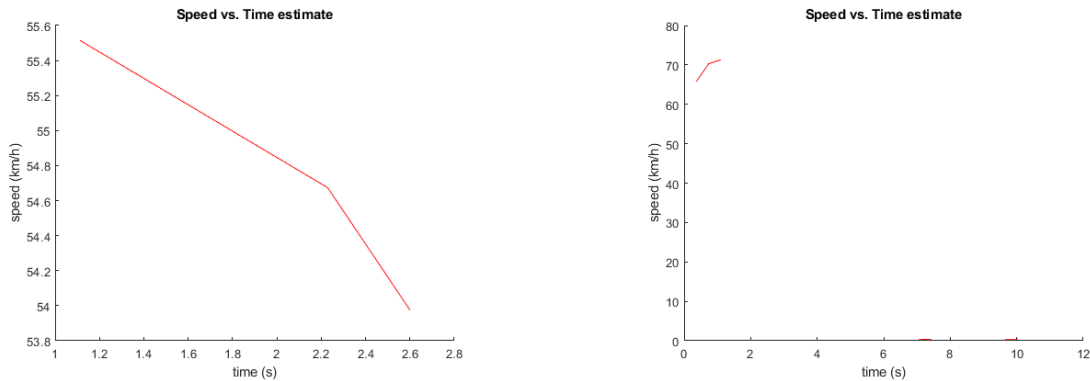
Table 6.2: Speed detection results for the Audi A1

The values found in Table.6.2 were considered accurate estimates as the Detected speeds were similar to that of the truth. The rest of the results were shown in B.1, Appendix B.

### 6.3.2 Lexus

The performance seen measured on the Lexus was recorded.

Speed approximations taken from Fig. 6.10 were displayed in Table. 6.3



(a) 05\_Bremner\_Lexus\_Driving\_Towards\_60KPH\_002.wav (b) 07\_Bremner\_Lexus\_Driving\_Towards\_80KPH\_001.wav

Figure 6.10: Final speed vs time plots derived from the applied algorithm on the Lexus

Fig.	Detected Speed	True Speed
6.10a	55.5km/h	60km/h
6.10b	73km/h	80km/h

Table 6.3: Speed detection results for the Lexus 4x4

The values found in Table.6.3 were considered near accurate estimates as the Detected speeds were close to that of the truth. It is noted that there is an almost constant offset between the true data and that which has been measured. From observation of the spectrogram, such as shown in Fig. 6.11 it can be seen that the issue likely is not from the CA-CFAR detection algorithm. It was also hypothesised that the data may have been measured at a slightly different centre frequency (fc),

road conditions may have caused inconsistency of the speedometer reading, or the speedometer may have been calibrated differently. The rest of the results were shown in [B.2](#), Appendix B.

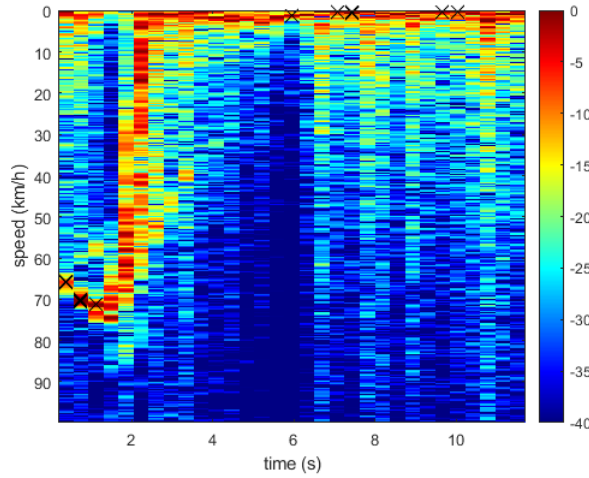


Figure 6.11: Spectrogram resulting from the measured signal of '07\_Bremner\_Lexus\_Driving\_Towards\_80KPH\_001.wav'

It was noted that the target locations, shown in Fig. [6.11](#), are seen to be accurate from sight, however based on the label it is wrong, this was consistent among all Lexus data sets.

### 6.3.3 Bike

The measurements were taken on a two-wheeled motorbike  
Speed approximations taken from Fig. [6.12](#) were displayed in Table. [6.4](#)

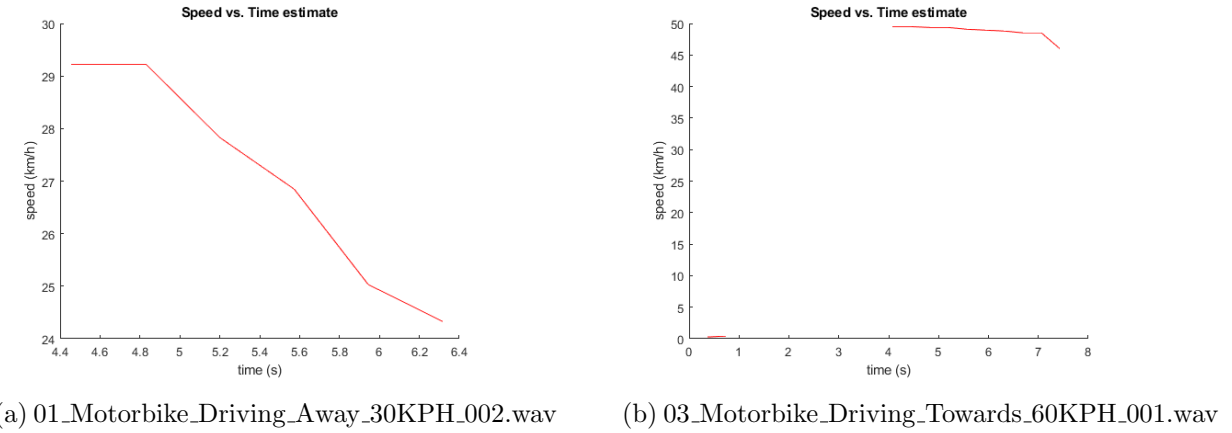


Figure 6.12: Final speed vs time plots derived from the applied algorithm on the Motorbike

Fig.	Detected Speed	True Speed
6.12a	29.2km/h	30km/h
6.12b	50km/h	60km/h

Table 6.4: Speed detection results for the motorbike

The values found in Table 6.4 were reasonably close to the true value for Fig. 6.12a. However, an offset was seen in deduced speed in Fig. 6.12b. In the spectrogram shown in Fig. 6.13, the target has been detected on what appears to be the signal of a higher power. Other, smaller lines were apparent at the specified speed value. The targets that were marked would, however, generally be seen as what should be considered the target based on the theory.

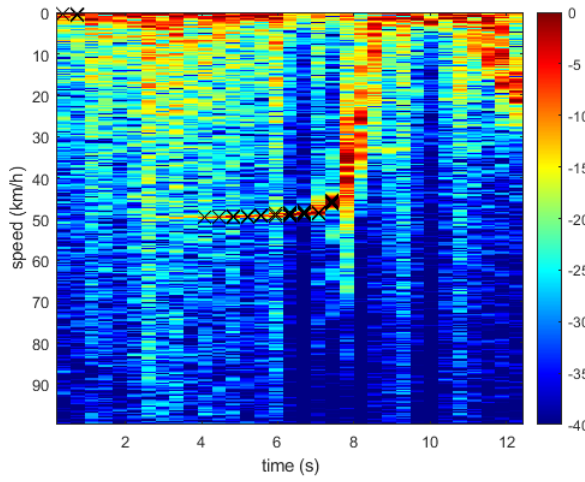


Figure 6.13: The spectrogram resulting from '03\_Motorbike\_Driving\_Towards\_60KPH\_001.wav'

This was observed to take place at higher speeds. It was noted that the RCS of a bike is the smallest of all data sets, however target detection was still achieved. The rest of the results were shown in [B.3](#), Appendix B.

### 6.3.4 Multi-target Detection

[CA-CFAR](#) processing has previously been shown not to perform on multiple target detection. When tested with the specified parameters the spectrograms shown in Fig. [6.14](#) we found. Since methodology to extract the speed from the spectrogram was designed with only one target in mind a specific speed value was not calculated.

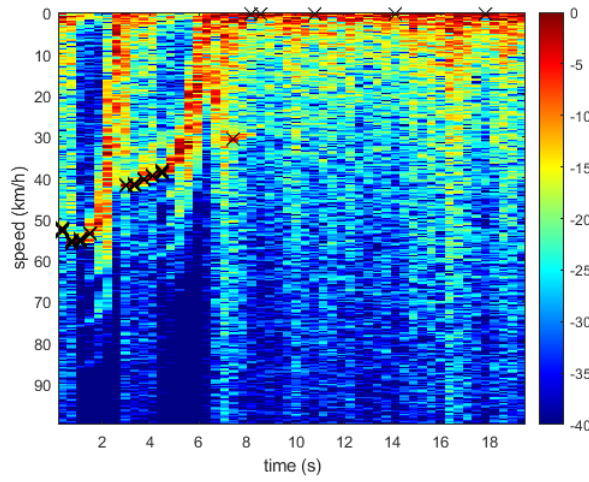


Figure 6.14: Spectrogram generated from '11\_Bremner\_Lexus\_InfrontOf\_PoloGtI\_\_Driving\_Towards\_60K'

As seen in Fig. 6.14 both targets were successfully spotted. However, since no specific speeds were detected, this has been deemed unsuccessful. The rest of the results were shown in B.4, Appendix B.

# Chapter 7

## Conclusions

### 7.1 Conclusions

In this report, optimising the input parameters used in the [STFT](#) and [CA-CFAR](#) processing were investigated.

Initially, code was constructed to perform the [STFT](#) and [CA-CFAR](#) processes. Validation was done which confirming that the code worked.

Target detections were made within an acceptable accuracy. Targets with a relatively smaller [RCS](#) were detected. Both in departure and arrival performance was seen to be mostly consistent. However a slightly better performance was seen in targets driving towards to the radar, this is explained to the higher signal power returned, as per Equation [2.2](#). The chosen parameter values that were tested have shown improvements in the performance of the [CA-CFAR](#)'s results.

It was observed that the speed estimations were accurate at speeds less than 45km/h. In some experiments, the estimated speeds were inaccurate, which were seen at higher speeds of above 50km/h. It was observed that the error was consistent between datasets, at  $\pm 10\text{km/h}$ . Further examination has shown that the targets detected were at positions accurate to the spectrograms seen. Conclusions attributing the reason for

the error to be associated with capturing the data, as the radar has measured it as the detected speed, however, data capturing was outside the scope of this report.

This report has also shown that there is a possibility of multi-target detection working with the CA-CFAR, which was not investigated as part of this project.

The work done has shown a noticeable improvement in limiting false alarms while still maintaining a suitable speed reading.

This research has determined that CA-CFAR signal processing provides suitable performance in traffic calming applications. However, improvements still need to be made to fully implement the use of a mobile S-band radar as a viable solution.

## 7.2 Future Work

Based on the results, it was seen that further investigation needs to take place in measuring the data. At higher speeds inaccuracies were seen concerning the frequency returned.

A method of automatically adapting input values to suit the environment can be researched.

Optimisation of other techniques in target detection can still be researched, and provide even better performance.

False alarms due to interference are expected, thus, implementations to disregard false alarms that don't fall within the expected target's behaviour can also be implemented.

There was also shown that a possibility exists for multi-target detection, this was not fully realised in the report, due to the system being unable to distinguish between the two targets. Thus, an algorithm that could realise this can be developed.

Further investigation could also be conducted in a more controlled way, allowing

for values such as target range to be known, aiding in calculations used in the investigation.

A more accurate true speed value would have also assisted in performing a more thorough evaluation on the results. A wider range of data sets would have assisted in evaluating trends seen in results.

Although decisions were made based on the theory, more in-depth theoretical research could have been conducted, focusing more in-depth on the aspects of radar such as target cross-sectional area, propagation effects and transmit gain, providing results which would propose better methods of data capturing.

# Bibliography

- [1] A. Ullah, S. Hussain, A. Wasim, and M. Jahanzaib, “Usage and impacts of speed humps on vehicles: A review,” *Journal of Advanced Review on Scientific Research*, vol. 28, pp. 1–17, 01 2016, (Accessed on 25/10/2021).
- [2] B. Mohit, Z. Rosen, and P. Muennig, “The impact of urban speed reduction programmes on health system cost and utilities,” *Injury Prevention*, vol. 24, pp. injuryprev–2017, 08 2017.
- [3] “Radarsign logo radar speed signs make roads safer request a quote today tc-1000 radar speed sign”,” <https://www.radarsign.com/radar-speed-signs/tc-1000-radar-speed-sign/>, 2021, (Accessed on 25/10/2021).
- [4] “Traffic signgs - repro supplies,” <https://reprosupplies.co.za/traffic-signs/>, 2021, (Accessed on 25/10/2021).
- [5] D. Vasilev, “Radar technology - a short history,” <https://www.skyradar.com/blog/brief-history-of-radar-technology>, 04 2019, (Accessed on 25/10/2021).
- [6] F. Najaar, “Mobile s-band radar testbed for traffic calming applications,” 2019, internal Report.
- [7] M. A. Richards, J. A. Scheer, and W. A. Holm, *Principles of modern radar*. Scitech Publishing Inc., 2015.

- [8] IEEE, “Ieee standard letter designations for radar-frequency bands,” *IEEE Std 521-1984*, pp. 1–8, 1984.
- [9] L. Colonel and P. Stathopoulos, “[c-uas] electromagnetic operations,” Jan 2021. [Online]. Available: <https://www.japcc.org/c-uas-electromagnetic-operations/>
- [10] R. M. O'Donnell. [Online]. Available: <https://www.youtube.com/playlist?list=PLUJAYadtuizA8RC2Qk8LfmiWA56HZsk9y>
- [11] Vortex, “Police radar: How radar works & how to beat speeding tickets,” Jul 2019. [Online]. Available: <https://www.vortexradar.com/2017/11/police-radar/>
- [12] R. Gao and R. Yan, “Non-stationary signal processing for bearing health monitoring,” *IJMR*, vol. 1, pp. 18–40, 01 2006.
- [13] J. O. Smith, *Spectral Audio Signal Processing*. <http://ccrma.stanford.edu/~jos/sasp/>, accessed jdatej, online book, 2011 edition.
- [14] G. Heinzel, A. Rüdiger, and R. Schilling, “Spectrum and spectral density estimation by the discrete fourier transform (dft), including a comprehensive list of window functions and some new flat-top windows,” *Max Plank Inst*, vol. 12, 01 2002.
- [15] I. M. Lockwood, “Ite traffic calming definition,” *Institute of Transportation Engineers. ITE Journal*, vol. 67, no. 7, p. 22, Jul. 1997.
- [16] G. Desai, V. Ambre, S. Jakharia, and S. Sherkhane, “Smart road surveillance using image processing,” pp. 1–5, 2018.
- [17] K. Kjemtrup and L. Herrstedt, “Speed management and traffic calming in urban areas in europe: a historical view.” *Accident; analysis and prevention*, vol. 24 1, pp. 57–65, 1992.

- [18] E. Blais and L. Carnis, "Improving the safety effect of speed camera programs through innovations: Evidence from the french experience," *Journal of safety research*, vol. 55, pp. 135–145, 2015.
- [19] J. Ambros, J. Novák, P. Neuwirth, M. Kieć, D. Dudek, T. Andriejauskas, and D. Skrodenis, "Using speed profiles to investigate the impact of traffic calming measures," 08 2017.
- [20] T. Vanderbilt, *Traffic: why we drive the way we do (and what it says about us)*. ALLEN LANE, 2008.
- [21] A. Dhar, "Traffic and road condition monitoring system," Bombay, Mumbai, India, 2008 [Online]. [Online]. Available: <https://citeseerx.ist.psu.edu/viewdoc/download?doi=10.1.1.518.2687&rep=rep1&type=pdf>
- [22] J. Lamas, P.-M. Castro-Castro, A. Dapena, and F. Vazquez-Araujo, "Sidivs: Simple detection of inductive vehicle signatures with a multiplex resonant sensor," *Sensors*, vol. 16, p. 1309, 08 2016.
- [23] D. Sawicki, "Police lidar operational problems," <https://copradar.com/chapts/chapt5/ch5d3.html>.
- [24] R. K. Jones and J. H. Lacey, "The effectiveness of laser and radar based enforcement programs for deterrence of speeding," U.S. Department of transport, 1997. [Online]. Available: <https://doi.org/10.21949/1404100>
- [25] S.-L. Jeng, W.-h. Chieng, and H.-P. Lu, "Estimating speed using a side-looking single-radar vehicle detector," *Intelligent Transportation Systems, IEEE Transactions on*, vol. 15, pp. 607–614, 04 2014.

- [26] D. Kellner, M. Barjenbruch, J. Klappstein, J. Dickmann, and K. C. J. Dietmayer, “Instantaneous ego-motion estimation using doppler radar,” *16th International IEEE Conference on Intelligent Transportation Systems (ITSC 2013)*, pp. 869–874, 2013.
- [27] M. A. Fischler and R. C. Bolles, “Random sample consensus: a paradigm for model fitting with applications to image analysis and automated cartography,” *Commun. ACM*, vol. 24, pp. 381–395, 1981.

# **Appendix A**

## **Code**

### **A.1 Code**

Github link to the full code used can be found [here](#).

# **Appendix B**

## **More Data sets**

The rest of the data sets can be seen here, provided as spectrograms, with Target detections at the X.

## B.1 Audi

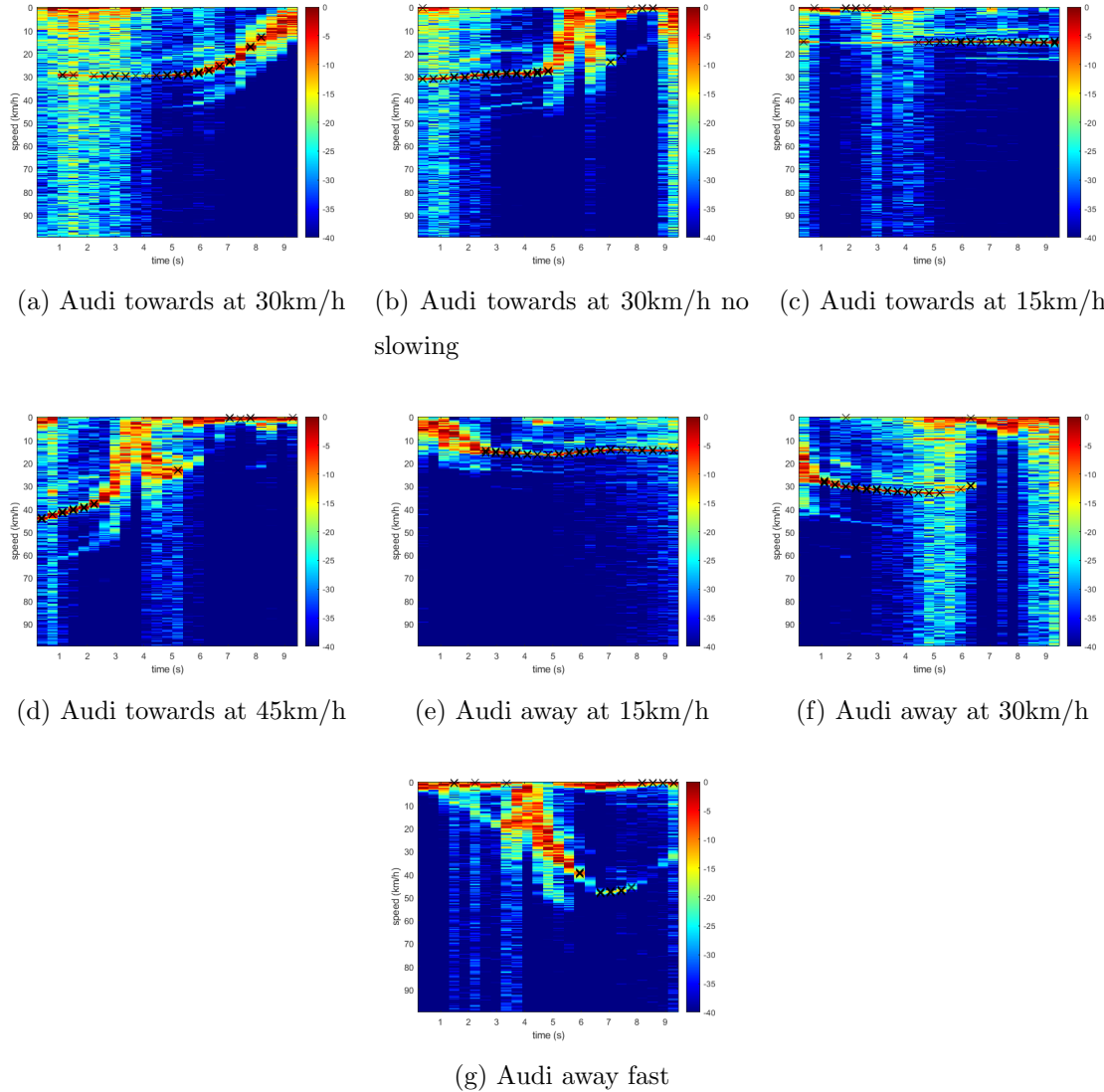


Figure B.1: Spectrograms generated from the Audi data set

## B.2 Lexus

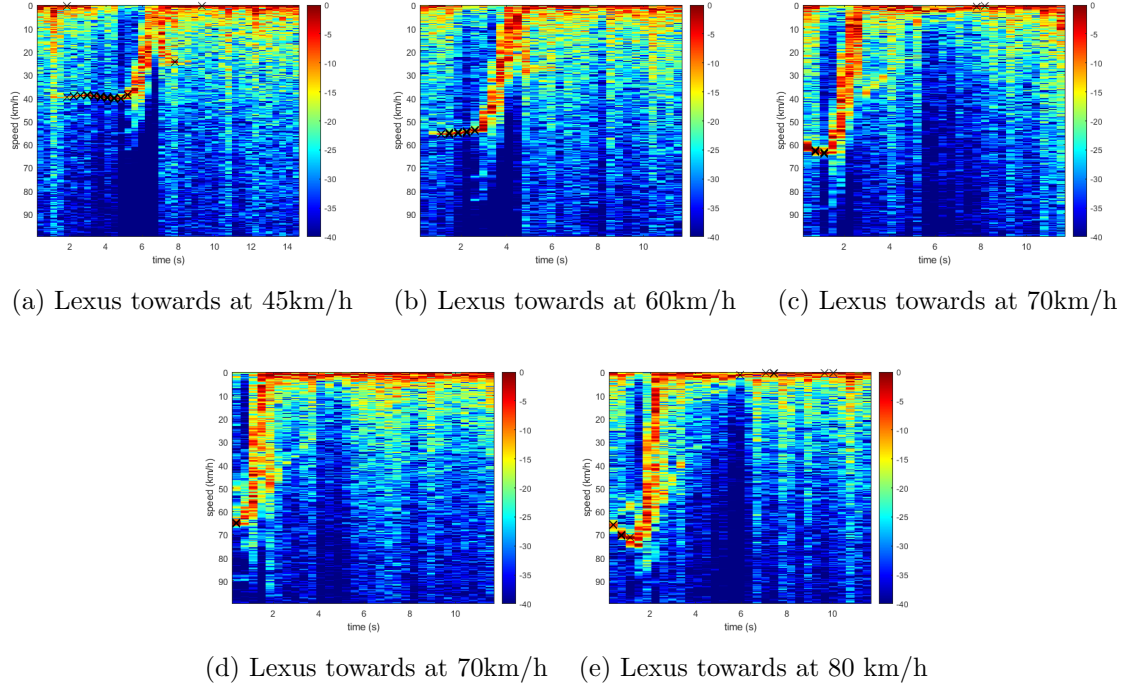
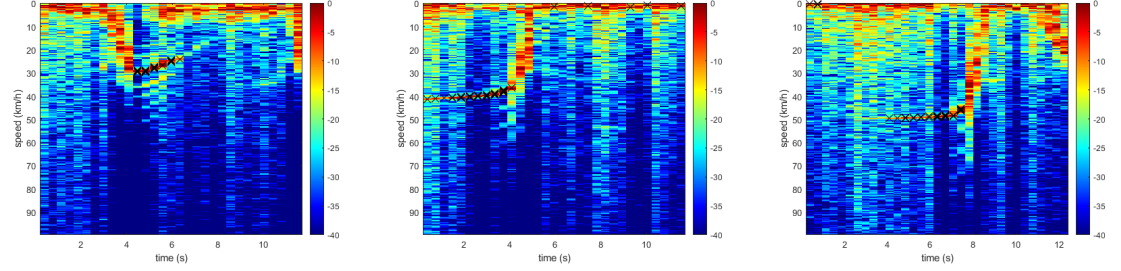


Figure B.2: All generated spectrograms of Lexus Bremner.

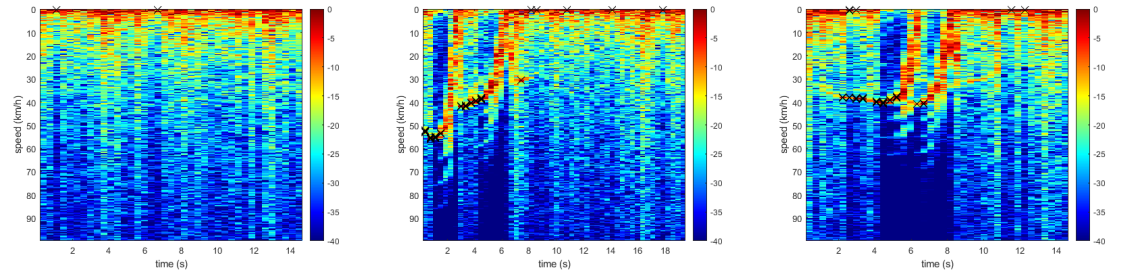
### B.2.1 Bike



(a) Bike driving away at 30km/h (b) Bike driving towards at 50km/h (c) Bike driving towards at 60km/h

Figure B.3: Spectrograms generated from the Bike data

### B.2.2 Multi-target



(a) Lexus and Polo GTI both at 30km/h (b) Lexus in front of Polo, towards at 45km/h (c) Lexus in front of GTI at 60km/h and 40km/h respectively

Figure B.4: Spectrograms generated from recordings when two vehicles passed

## ETHICS APPLICATION FORM

**Please Note:**

Any person planning to undertake research in the Faculty of Engineering and the Built Environment (EBE) at the University of Cape Town is required to complete this form **before** collecting or analysing data. The objective of submitting this application *prior* to embarking on research is to ensure that the highest ethical standards in research, conducted under the auspices of the EBE Faculty, are met. Please ensure that you have read, and understood the **EBE Ethics in Research Handbook** (available from the UCT EBE, Research Ethics website) prior to completing this application form: <http://www.ebe.uct.ac.za/ebe/research/ethics1>

<b>APPLICANT'S DETAILS</b>			
Name of principal researcher, student or external applicant		Salmaan Kamaloodien	
Department		Engineering and the Built Environment	
Preferred email address of applicant:		KMLSAL001@myuct.ac.za	
If Student	Your Degree: e.g., MSc, PhD, etc.	Bsc Mechatronics Engineering	
	Credit Value of Research: e.g., 60/120/180/360 etc.	40	
	Name of Supervisor (if supervised):	Dr. Yunus Abdul Gaffar	
If this is a researchcontract, indicate the source of funding/sponsorship			
Project Title		YAG21-03 Radar signal and data processing for traffic calming radar applications	

**I hereby undertake to carry out my research in such a way that:**

- there is no apparent legal objection to the nature or the method of research; and
- the research will not compromise staff or students or the other responsibilities of the University;
- the stated objective will be achieved, and the findings will have a high degree of validity;
- limitations and alternative interpretations will be considered;
- the findings could be subject to peer review and publicly available; and
- I will comply with the conventions of copyright and avoid any practice that would constitute plagiarism.

<b>APPLICATION BY</b>	Full name	Signature	Date
<b>Principal Researcher/ Student/External applicant</b>	Salmaan Kamaloodien		2021/08/14
<b>SUPPORTED BY</b>	Full name	Signature	Date
<b>Supervisor (where applicable)</b>	Dr M. Y. Abdul Gaffar		16/08/2021

<b>APPROVED BY</b>	Full name	Signature	Date
<b>HOD (or delegated nominee)</b>  Final authority for all applicants who have answered NO to all questions in Section 1; and for all Undergraduate research (Including Honours).			
<b>Chair: Faculty EIR Committee</b>  For applicants other than undergraduate students who have answered YES to any of the questions in Section 1.			